Seiches: a tale of misconceptions?

Eric Deleersnijder, 3 September 2024 - 28 November 2024

Contents

Abstract. The governing equations of a non-dissipative, two-layer hydrodynamic model are linearised. Following classical textbooks, the equations of the external mode and that of the internal one are established. Then, the related inertia gravity waves are briefly studied. Next, in an idealised, one-dimensional lake, external and internal seiches (i.e., free oscillations) are modelled, underscoring the fact that the timescale of the external mode is much smaller than that of the internal one. Under simple initial conditions, the surface and thermocline displacements are seen to be continuous piecewise linear functions in space exhibiting oscillations in time, which are best understood in the framework of the theory of distributions. On the other hand, the response to an abruptly imposed wind forcing leads to solutions of the same nature, which might not be fully in accordance with common knowledge about seiching motions. Volume and mechanical energy conservation are dealt with in Appendix A. We also briefly investigate the impact of vertical discretisation on the propagation of hydrostatic internal waves in level models (Appendix B).

Motivation

Ishimwe (2023, 2024, 2025) greatly improved the time stepping of SLIM (www.slim-ocean.be), which, among other things, includes a novel approach to the mode splitting. This entails treating in a different manner the external mode and the internal one. Presumably, this numerical technique was introduced in the seventies (Gadd 1978). It has been used and improved by many authors since then (e.g., Blumberg and Mellor 1987, Killworth et al. 1991, Higdon and de Szoeke 1997, Shchepetkin and McWilliams 2005, Vallaeys et al. 2018).

Hereinafter, a linearised, two-layer, non-dissipative model is put forward. Such a model is aimed at taking into account the effect of stratification in (what presumably is) the most elementary manner. Needless to say, there exist more realistic approaches to the impact of stratification. If the density is a continuous function (instead of a discontinuous one) of the vertical coordinate, linearised equations lead to solutions consisting of a sum of modes (e.g., Moore and Philander 1977, Chapter 3 of LeBlond and Mysak 1978). The semi-discretised version of these equations (discretisation along the vertical direction only) also admits analytical solutions, allowing for the comparison of the internal wave speed obtained in the continuous model and with that of the semi-discrete one (e.g., Deleersnijder 1992).

Hereinafter, analytical solutions are derived for an idealised geometry, which pertain to plane waves in an unbounded domain, one-dimensional seiches and wind-induced motion. In the first two test cases, the external mode and the internal one evolve independently of each other, whereas, in the third type of flow, the external and internal modes are linked through the wind forcing. These theoretical results, which are loosely inspired by Chapter 12 of Cushman-Roisin and Beckers (2011), might be instrumental in assessing some aspects of SLIM's newly developed code. As for the values of key parameters, some inspiration was sought in studies of Lake Tanganyika (e.g., Coulter and Spigel 1991, Naithani et al. 2002, Naithani et al. 2003), Lake Kinneret (van Emmerik et al. 2013), Lake Constance (e.g., Wahl and Peeters 2014) or Lake Baikal (e.g., Piccolroaz and Toffolon 2018).

Two-layer model

Consider two layers of homogeneous fluid separated by a sharp pycnocline, which is assumed to be completely impermeable (Figure 1). The superscript "*s*" refers to the surface layer, whilst "*b*" is associated with the bottom layer. The density in the surface (resp. bottom) layer is constant ρ^s (resp. ρ^b). The elevation of the free surface (positive upward) is denoted η. The downward displacement of the pycnocline is ξ. If these surfaces are at their reference position, the height of the surface (resp. bottom) layer reads h^s (resp. h^b). The actual heights of these layers are $H^s = h^s + \eta + \xi$ and $H^b = h^b - \xi$. The (horizontal) velocities are denoted $\mathbf{u}^s$ and $\mathbf{u}^b$, whilst the corresponding transports are $\mathbf{U}^s = H^s\mathbf{u}^s$ and $\mathbf{U}^b = H^b\mathbf{u}^b$.

The flow is governed by Saint-Venant equations in both layers, i.e.,

$$\partial_t(\eta+\xi) \;+\; \nabla\bullet\mathbf{U}^s \;=\; 0 \tag{1}$$

$$\rho^s\left[\partial_t\mathbf{U}^s + \nabla\bullet\left(\mathbf{U}^s\mathbf{U}^s / H^s\right) + f\,\mathbf{e}_z\times\mathbf{U}^s\right] \;=\; -g\rho^s H^s\nabla\eta \;+\; \boldsymbol{\tau}^s \tag{2}$$

$$\partial_t(-\xi) \;+\; \nabla\bullet\mathbf{U}^b \;=\; 0 \tag{3}$$

$$\rho^b\left[\partial_t\mathbf{U}^b + \nabla\bullet\left(\mathbf{U}^b\mathbf{U}^b / H^b\right) + f\,\mathbf{e}_z\times\mathbf{U}^b\right] \;=\; -g\rho^b H^b\nabla\eta \;+\; g(\rho^b-\rho^s)H^b\,\nabla(\eta+\xi) \tag{4}$$

where $\nabla = (\partial_x, \partial_y)$ denotes the "horizontal part" of the del operator; constants $g \approx 9.81$ m/s^2 and *f* are the gravitational acceleration and the Coriolis parameter, respectively; $\mathbf{e}_z$ represents a unit vertical vector, pointing upward; $\boldsymbol{\tau}^s$ is the stress exerted by the wind on the water-air interface. Obviously, (1) and (3) are the continuity equations for the upper layer and the lower one, respectively, whilst the horizontal momentum for these layers are equations (2) and (4).

Equations (1)-(4) are obtained by integrating over the vertical direction the three-dimensional, hydrostatic Navier-Stokes equations. All turbulent fluxes are disregarded, except that related to the wind stress, thereby allowing surface forcing, if need be (e.g., Csanady 1982). To the best of the author's knowledge, there exists no analytical solutions to these equations. However, highly accurate numerical solutions of them can be obtained (e.g., Vreugdenhil 1994) and their energy budget may be examined (see Appendix A).

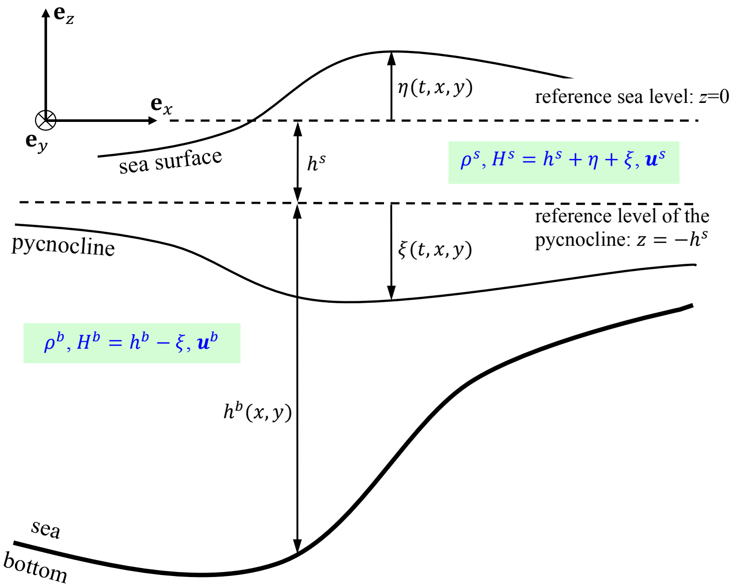

Figure 1. Vertical section through the water body of interest showing the main variables and parameters.

Linearised equations

Assume that the reference height of the bottom layer, h^b, is constant. If the initial conditions and the surface forcing are such that (1)-(4) can be linearised, then one obtains the following linear partial differential equations (with constant coefficients)

$$\partial_t(\eta+\xi) + \nabla \bullet \mathbf{U}^s = 0 \tag{5}$$

$$\partial_t \mathbf{U}^s + f\,\mathbf{e}_z \times \mathbf{U}^s = -gh^s\nabla\eta + \frac{\boldsymbol{\tau}^s}{\rho^s} \tag{6}$$

$$\partial_t(-\xi) + \nabla \bullet \mathbf{U}^b = 0 \tag{7}$$

$$\partial_t \mathbf{U}^b + f\,\mathbf{e}_z \times \mathbf{U}^b = -gh^b\nabla\eta + gh^b\varepsilon\nabla(\eta+\xi) \tag{8a}$$

where

$$\varepsilon = \frac{\rho^b - \rho^s}{\rho^b} << 1 \tag{9}$$

denotes the relative density difference between the two fluid layers under consideration. This parameter is sufficiently small that, in (8a), $gh^b\varepsilon\nabla(\eta+\xi)$ is generally significantly smaller than $gh^b\nabla\eta$. For most applications, it may be assumed that $10^{-3} \lesssim \varepsilon \lesssim 10^{-2}$.

The air density, ρ^a, is much smaller than the water density ($\rho^a / \rho^s \approx 10^{-3}$). Consider a fluid parcel of volume δV located at the surface of the water body. The work needed to vertically move this fluid parcel over distance δz tends to $g(\rho^s - \rho^a)\delta z\delta V \approx g\rho^s\delta z\delta V$ in the limit $\delta z, \delta V \to 0$. On the other hand, the work needed to vertically move a fluid parcel located at the upper boundary of the lower layer over distance δz tends to $g(\rho^b - \rho^s)\delta z\delta V$ in the limit $\delta z, \delta V \to 0$. Clearly, the latter work is much smaller than the former, which is the reason why the pycnocline displacement can be much larger than that of the free surface of the water body, i.e., $|\eta| << |\xi|$. Therefore, the last term in the right-hand side of (8a) may be simplified to $gh^b\varepsilon\nabla\xi$, allowing rewriting (8a) as follows

$$\partial_t \mathbf{U}^b + f\mathbf{e}_z \times \mathbf{U}^b = -gh^b\nabla\eta + gh^b\varepsilon\nabla\xi \tag{8b}$$

External and internal mode equations

The external mode transport and water height are

$$\mathbf{U} = \mathbf{U}^s + \mathbf{U}^b = h^s\mathbf{u}^s + h^b\mathbf{u}^b \tag{10}$$

and

$$h = h^s + h^b \tag{11}$$

Taking the sum of (5) and (7) on the one hand and (6) and (8b) on the other hand (and neglecting $gh^b\varepsilon\nabla\xi$ because of the smallness of ε) yields the continuity and horizontal momentum equations of the external mode, i.e.,

$$\partial_t \eta + \nabla \bullet \mathbf{U} = 0 \tag{12}$$

$$\partial_t \mathbf{U} + f\mathbf{e}_z \times \mathbf{U} = -gh\nabla\eta + \frac{\boldsymbol{\tau}^s}{\rho^s} \tag{13}$$

which obviously are classical, linearised shallow-water (or Saint-Venant) equations for a water column of constant depth h.

The internal mode transport may be defined to be

$$\mathbf{U}' = \frac{h^b\mathbf{U}^s - h^s\mathbf{U}^b}{h} = h'(\mathbf{u}^s - \mathbf{u}^b) \tag{14}$$

with

$$h' = \frac{h^s h^b}{h} \tag{15}$$

Manipulating (5)-(8b) so as to focus on the internal mode leads to

$$\partial_t \xi + \nabla \bullet \mathbf{U}' = 0 \tag{16}$$

$$\partial_t \mathbf{U}' + f\,\mathbf{e}_z \times \mathbf{U}' = -g' h' \nabla \xi + \frac{h^b \boldsymbol{\tau}^s}{\rho^s h} \tag{17}$$

where

$$g' = \varepsilon g \tag{18}$$

is commonly termed "reduced gravitational acceleration". Equations (16)-(17) may be seen as shallow-water equations related to a water column of depth h' and gravitational acceleration g'.

If the surface layer is much thinner than the bottom one $(h^s << h^b)$, then (16)-(17) simplifies to "reduced-gravity model" equations, i.e.,

$$\partial_t \xi + \nabla \bullet \mathbf{U}^s = 0 \tag{19}$$

$$\partial_t \mathbf{U}^s + f\,\mathbf{e}_z \times \mathbf{U}^s = -g' h^s \nabla \xi + \frac{\boldsymbol{\tau}^s}{\rho^s} \tag{20}$$

This is chiefly because $h' \sim h^s$ and $h^b \sim h$ in the limit $h^s / h^b \to 0$. Equations (19)-(20) contain parameters and variables related only to the surface layer, implying that the dynamics of this layer may be tackled without explicitly taking into account the processes developing in the bottom layer. A similar line of reasoning also holds valid for equations that have not been linearised (e.g., Naithani et al. 2002).

Some claim that the reduced-gravity model equations may be derived by simply assuming that the bottom layer is motionless. The above considerations show that this belief is somewhat misleading. Clearly, the arguments leading to (19)-(20) are somewhat subtler.

External and internal inertia gravity waves

Assume that the wind stress is zero $(\boldsymbol{\tau}^s = 0)$, implying that only unforced motion will be dealt with. If the domain is unbounded, i.e., $(x,y) \in \mathbb{R}^2$, then the external mode can take the form of a plane wave,

$$\begin{bmatrix} \eta(t,x,y) \\ \mathbf{U}(t,x,y) \end{bmatrix} = \mathrm{Re}\left[\begin{pmatrix} \mathcal{E} \\ \mathcal{V} \end{pmatrix} e^{i(\omega t - \mathbf{k} \bullet \mathbf{x})} \right] \tag{21}$$

where Re is the operator yielding the real part of a complex function; $\mathcal{E}$ and $\mathcal{V}$ are complex constant; $i = \sqrt{-1}$; ω is the angular frequency; $\mathbf{k} = (k,l)$ is the wavenumber vector and $\mathbf{x} = (x,y)$ is the horizontal part of the position-vector. Next, substituting (21) into (12)-(13) yields the following system of algebraic equations[1]

$$\begin{cases} i\omega \mathcal{E} - i\mathbf{k} \bullet \mathcal{V} = 0 \\ i\omega \mathcal{V} + f\mathbf{e}_z \times \mathcal{V} = igh\mathbf{k}\mathcal{E} \end{cases} \tag{22}$$

After some calculations, the momentum equation leads to

[1] An alternative approach consists in first manipulating (12)-(13) so as to derive the equation governing the evolution of the surface elevation, i.e., $\partial_t \left(\partial_{tt} \eta + f^2 \eta - gh \nabla^2 \eta \right) = 0$ (e.g., LeBlond and Mysak 1978). Then, by substituting a plane wave solution similar to (21) into this equation, we readily obtain (24).

$$\mathcal{V} = \frac{gh}{\omega^2 - f^2}(\omega\mathbf{k} + if\mathbf{e}_z \times \mathbf{k})\,\mathcal{E} \tag{23}$$

Then, combining the continuity equation in (22) with (23) leads to

$$i\omega\left(1 - \frac{g|\mathbf{k}|^2}{\omega^2 - f^2}\right)\mathcal{E} = 0 \tag{24}$$

Therefore, for a non-trivial solution of (22) to exist ($\mathcal{V} \neq 0, \mathcal{E} \neq 0$), it is necessary that $\omega = 0$, which corresponds to the geostrophic equilibrium (and, hence, is uninteresting in the present developments, for one is looking for a wave solution), or that

$$\omega^2 = f^2 + gh|\mathbf{k}|^2 \tag{25}$$

which is the well-known dispersion relation of Poincaré (or inertia-gravity) waves. Their angular frequency is always larger than the Coriolis parameter, f. Their phase speed, $\mathbf{C}_p \triangleq \omega|\mathbf{k}|^{-2}\,\mathbf{k}$, satisfies

$$|\mathbf{C}_p| = \sqrt{gh}\,\sqrt{1 + \frac{|\mathbf{k}|^{-2}}{R^2}} \tag{26}$$

where the length scale

$$R = \frac{\sqrt{gh}}{|f|} \tag{27}$$

is the external Rossby radius of deformation. The inverse (of the norm) of the wavenumber may be viewed as the length scale L of the wave under consideration, i.e., $L = 1/|\mathbf{k}|$. Accordingly, (26) may be rewritten as follows

$$|\mathbf{C}_p| = \sqrt{gh}\,\sqrt{1 + \frac{L^2}{R^2}} \tag{28}$$

Therefore, the phase speed of relatively short waves (i.e., waves whose length scale is much shorter than R), admits the following asymptotic expression

$$|\mathbf{C}_p| \sim \sqrt{gh}\left(1 + \frac{L^2}{2R^2}\right), \quad \frac{L}{R} \to 0 \tag{29}$$

Obviously, similar developments may be achieved for the internal mode, leading to the following dispersion relation

$$(\omega')^2 = f^2 + g'h'|\mathbf{k}|^2 \tag{30}$$

The associated phase speed reads

$$|\mathbf{C}'_p| = \sqrt{g'h'}\,\sqrt{1 + \frac{|\mathbf{k}|^{-2}}{(R')^2}} \tag{31}$$

where

$$R' = \frac{\sqrt{g'h'}}{|f|} \tag{32}$$

is the internal Rossby radius of deformation. The latter is much smaller than its external counterpart (Figure 2): roughly speaking, the external Rossby radius of deformation is one to two orders of magnitude greater than its internal counterpart.

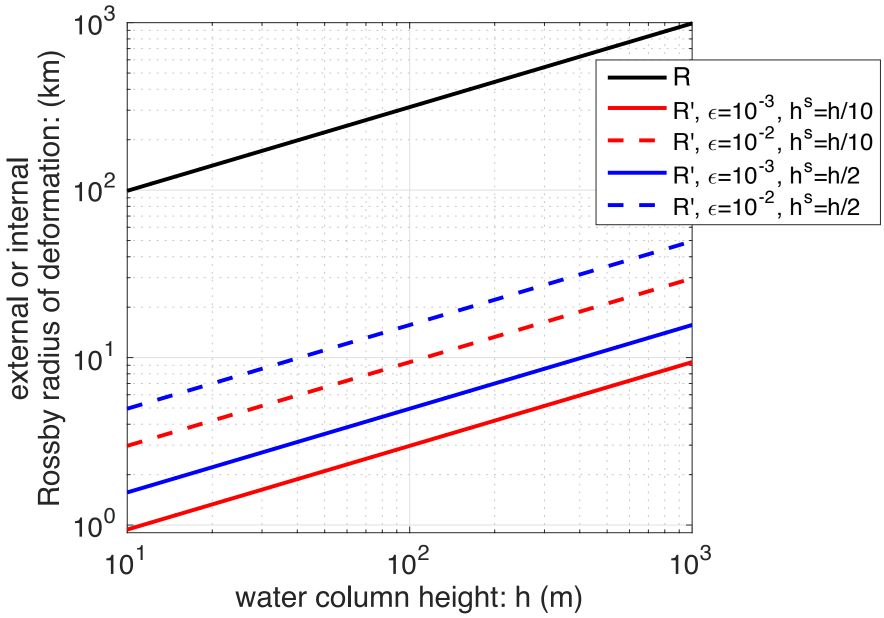

Figure 2. External and internal Rossby radius of deformation, i.e., $R = \sqrt{gh}\ /|f|$ and $R' = \sqrt{g'h'}\ /|f|$, respectively, as a function of the reference water depth (h) and for several values of ε and h^s / h.

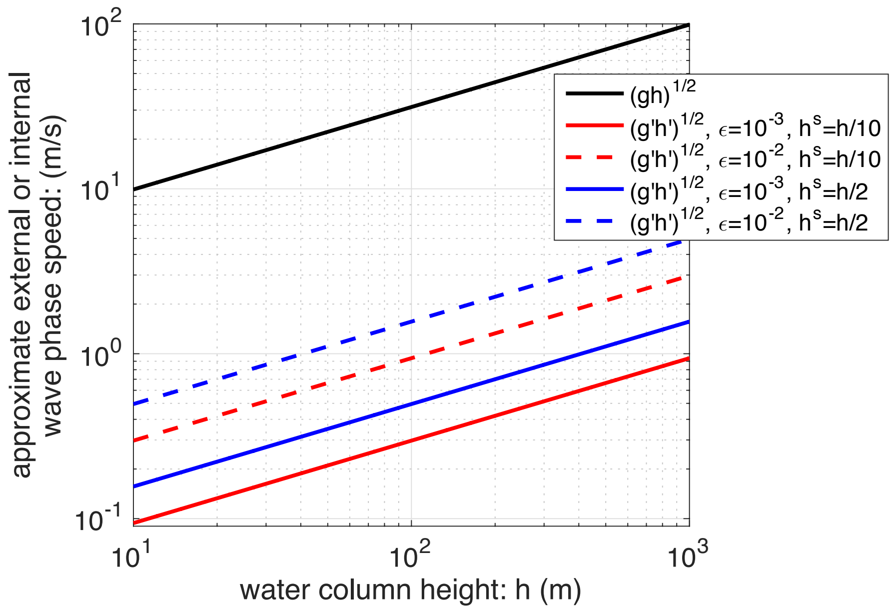

Figure 3. Approximate external and internal wave phase speed, i.e., $\sqrt{gh}$ and $\sqrt{g'h'}$, respectively, as a function of the reference water depth (h) and for several values of ε and h^s / h.

External waves of physical relevance are likely to be characterised by length scales ($L = |\mathbf{k}|^{-1}$) much smaller than the external Rossby radius. This is why $\sqrt{gh}$ is a (very) good approximation of their phase speed (Figure 3). Similar considerations apply to internal waves, albeit to a lesser degree. Accordingly, only $\sqrt{g'h'}$ is displayed in Figure 3. The phase speed of external waves is one to two orders of magnitude greater than their internal counterparts.

Using the von Neumann analysis (e.g., Crank and Nicolson 1947, Isaacson and Keller 1966) it is possible to assess numerical schemes aimed at representing external and internal inertia-gravity waves on regular grids (e.g., Mesinger and Arakawa 1976, Beckers and Deleersnijder 1993, Le Roux 2012) or irregular ones (e.g., Bernard et al. 2008). Remarkably, the internal wave phase speed may be greater than the norm of the water velocity, which has to be taken into account when analysing the properties of numerical schemes for the internal modes, in particular their stability.

External and internal seiches

In the words of Baretta-Bekker et al. (1998), a seiche[2] is a "standing wave occurring in lakes or in semi-enclosed embayments as a result of some sudden disturbance". This definition applies to external or internal seiches, i.e., the displacement of the water-air interface or the pycnocline, respectively. For instance, seiches frequently take place in the port of Rotterdam (e.g., de Jong et al. 2003, de Jong and Battjes 2004), the American Great Lakes (e.g., Trebitz 2066), Lake Baikal (e.g., Smirnov et al. 2014) or the Adriatic Sea (e.g., Cerovecki 1997, Bajo et al. 2019). On the other hand, in September 2023, a rockslide caused a major seiching event in a Greenland fjord (Svennevig et al., 2024).

Consider a one-dimensional, linearised, two-layer model of a lake[3] of length $L = 200$ km and depth $h = 200$ m . Then, the governing equations of the external mode are

$$\partial_t \eta + \partial_x U = 0 \tag{33}$$

$$\partial_t U = -gh\, \partial_x \eta \tag{34}$$

where $x \in [-L/2, L/2]$ denotes the along-lake coordinate. The ends of the lake are impermeable:

$$\left[U(t,x)\right]_{x=\pm L/2} = 0 \tag{35}$$

At the initial time, the lake is assumed to be motionless, i.e.,

$$\left[U(t,x)\right]_{t=0} = 0 \tag{36}$$

whilst the initial surface elevation is

$$\left[\eta(t,x)\right]_{t=0} = \eta_0(x) \tag{37}$$

which, in line with the concept of seiche, is assumed to satisfy $\eta_0(x) = -\eta_0(-x)$.

The solution to partial differential problem (33)-(37) reads

[2] The etymology of the word "seiche" seems to be rather obscure. Apparently, it was first used in the 19th century in Swiss French to "describe the rise and fall of water in Lake Geneva". Source: https://www.wordreference.com/definition/seiche (last viewed on 14 July 2024). See also Forel (1876).

[3] In most, if not all lakes, density contrasts are due to temperature variations. Hence, the pycnocline, if any, could be referred to as the thermocline. However, for the sake of generality, the word "pycnocline" will be used throughout the present working note.

$$\eta(t,x) = \sum_{n=1}^{\infty} E_n \cos(\omega_n t)\sin(k_n x) \tag{38}$$

$$U(t,x) = -\sqrt{gh}\sum_{n=1}^{\infty} E_n \sin(\omega_n t)\cos(k_n x) \tag{39}$$

with $k_n = (2n-1)\pi / L$, $\omega_n = \sqrt{gh}\; k_n$ and

$$E_n = \frac{2}{L}\int_{-L/2}^{L/2} \eta_0(x)\sin(k_n x)\,dx \tag{40}$$

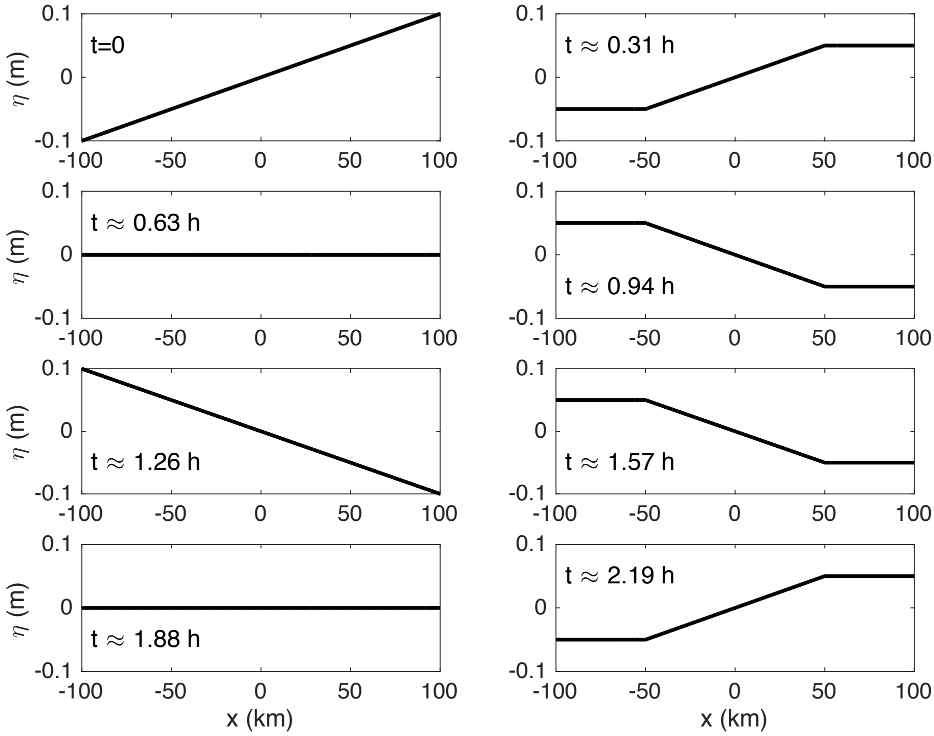

Figure 4. Seiching motion of lake surface elevation $\eta(t,x)$ according to (38) and (44). The length and depth of the lake are $L = 200$ km and $h = 200$ m, respectively. The period of the external seiche represented here is approximately 2.51 hours.

Obviously, (38) and (39) represent standing waves. They may also be viewed as the sum of non-dispersive waves travelling at phase speed $\sqrt{gh}$ in opposite directions, i.e.,

$$\eta(t,x) = \frac{1}{2}\sum_{n=1}^{\infty} E_n\left[\sin\left[k_n(x-\sqrt{gh}\;t)\right]+\sin\left[k_n(x+\sqrt{gh}\;t)\right]\right] \tag{41}$$

$$U(t,x) = \frac{\sqrt{gh}}{2}\sum_{n=1}^{\infty} E_n\left[\sin\left[k_n(x-\sqrt{gh}\;t)\right]-\sin\left[k_n(x+\sqrt{gh}\;t)\right]\right] \tag{42}$$

The elevation and transport are periodic functions of time, the period being that of the first oscillatory mode $(n=1)$, i.e.,

$$\tau_1 = \frac{2\pi}{\omega_1} = \frac{2L}{\sqrt{gh}} \approx 2.51 \text{ hours} \tag{43}$$

Unsurprisingly, this is the time needed to travel at speed $\sqrt{gh}$ from one end of the lake to the other and back. Accordingly, the elevation and transport satisfy $\eta(t,x) = \eta(t+\tau_1,x)$ and $U(t,x) = U(t+\tau_1,x)$.

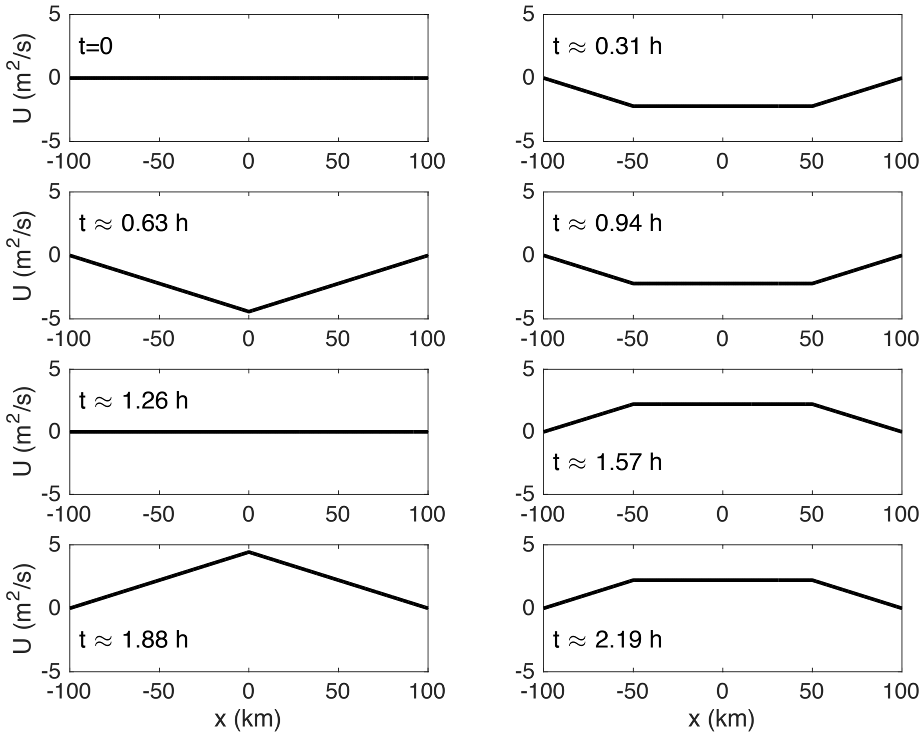

Figure 5. Transport $U(t,x)$ obtained from (39) and (44). This variable is related to the external seiche whose surface displacement is displayed in Figure 4.

The simplest initial elevation profile probably is $\eta_0(x) = (2x/L)E$, leading to

$$E_n = \frac{8(-1)^{n+1}}{\pi^2(2n-1)^2} E \tag{44}$$

The maximum amplitude of the seiching displacement of the surface occurs at the ends of the lake and is equal to $|E|$. For $E = 0.1\,\text{m}$, Figures 4 and 5 represent the surface elevation and the transport at $t = 0, \tau_1/8, 2\tau_1/8, \ldots 7\tau_1/8$.

The governing equations of the internal mode are

$$\partial_t \xi + \partial_x U' = 0 \tag{45}$$

$$\partial_t U' = -g'h' \partial_x \xi \tag{46}$$

The ends of the lake are impermeable:

$$[U'(t,x)]_{x=\pm L/2} = 0 \tag{47}$$

At the initial time, the lake is assumed to be motionless, i.e.,

$$\left[U'(t,x)\right]_{t=0} = 0 \tag{48}$$

whilst the initial surface elevation is

$$\left[\xi(t,x)\right]_{t=0} = \xi_0(x) \tag{49}$$

which, in line with the concept of seiche, is assumed to satisfy $\xi_0(x) = -\xi_0(-x)$.

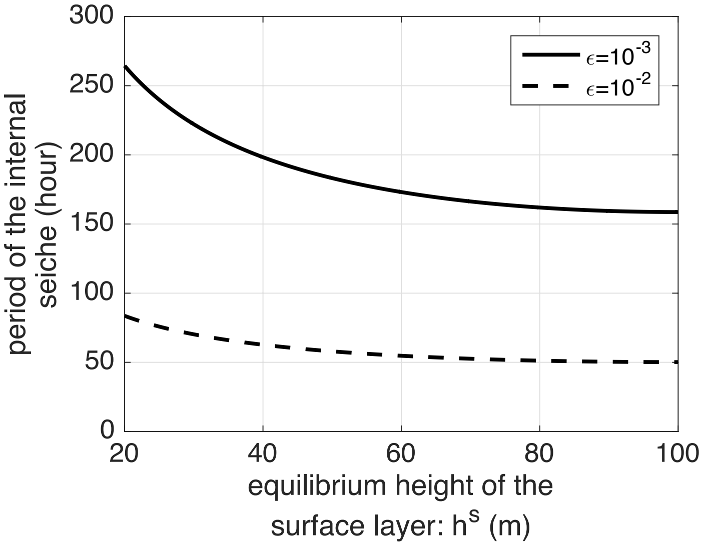

Figure 6. Period of the internal seiche in the one-dimensional lake 200 km in length and 200 m in depth. The ratio of the surface layer height (h^s) to the total depth ranges from $1/10$ (i.e., $h^s = 20$ m) to $1/2$ (i.e., $h^s = 100$ m). Two values of the relative density difference (ε) are taken into consideration: they represent the lowest and largest values that are likely to be encountered *in situ*. It must be kept in mind that the period of the external seiche (i.e., approximately 2.51 hours) is much shorter than the period of any internal seiche.

The solution to partial differential problem (45)-(49) obviously bears similarities with that governing the external seiche, and is as follows

$$\xi(t,x) = \sum_{n=1}^{\infty} \Xi_n \cos(\omega'_n t)\sin(k_n x) \tag{50}$$

$$U'(t,x) = -\sqrt{g'h'} \sum_{n=1}^{\infty} \Xi_n \sin(\omega'_n t)\cos(k_n x) \tag{51}$$

with $k_n = (2n-1)\pi / L$, $\omega'_n = \sqrt{g'h'}\, k_n$ and

$$\Xi_n = \frac{2}{L} \int_{-L/2}^{L/2} \xi_0(x)\sin(k_n x)\, dx \tag{52}$$

Obviously, (50) and (51) represent standing waves. They may also be viewed as the sum of non-dispersive waves travelling at phase speed $\sqrt{g'h'}$ in opposite directions. The internal seiche is periodic. Its period is that of the first oscillatory mode $(n = 1)$ (Figure 6)

$$\tau_1' = \frac{2\pi}{\omega_1'} = \frac{2L}{\sqrt{g'h'}} \tag{53}$$

Unsurprisingly, this is the time needed to travel at speed $\sqrt{g'h'}$ from one end of the lake to the other and back. Accordingly, the pycnocline displacement and internal mode transport satisfy $\xi(t,x) = \xi(t+\tau_1',x)$ and $U'(t,x) = U'(t+\tau_1',x)$. For a given value of ε, the minimum of the period of the internal seiche is $4L/\sqrt{g'h}$; it occurs for $h^s = h^b = h/2$.

The simplest initial pycnocline displacement profile probably is $\xi_0(x) = (2x/L)\Xi$, leading to

$$\Xi_n = \frac{8(-1)^{n+1}}{\pi^2(2n-1)^2}\,\Xi \tag{54}$$

The maximum amplitude of the seiching displacement of the pycnocline occurs at the ends of the lake and is equal to $|E|$. For $\Xi = 1\,\mathrm{m}$, Figure 7 displays the position of the pycnocline $(-\xi)$ at $t = 0, \tau_1/8, 2\tau_1/8, \ldots 7\tau_1/8$.

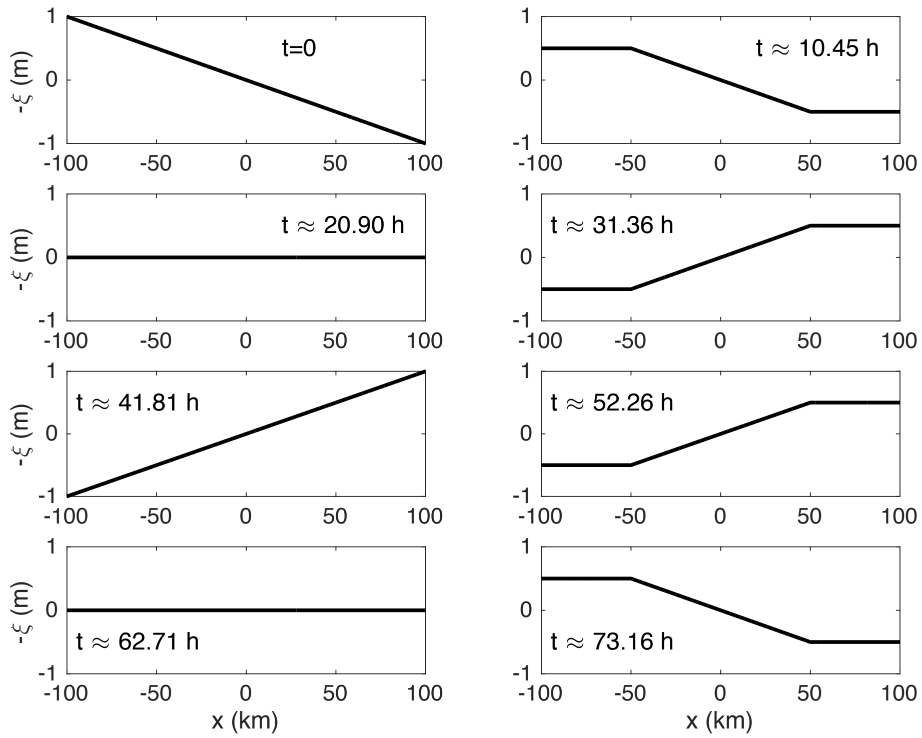

Figure 7. Seiching motion of the pycnocline according to expressions (50) and (54). The length and depth of the lake are $L = 200\,\mathrm{km}$ and $h = 200\,\mathrm{m}$, respectively. The relative density difference is $\varepsilon = 10^{-2}$, whilst the reference surface layer height is $h^s = h/10 = 20\,\mathrm{m}$. The period of this internal seiche is approximately 83.62 hours.

Solutions in the sense of distributions

By combining (33)-(34), it is readily seen that the elevation and transport satisfy the following canonical wave (or hyperbolic) equations

$$\partial_{tt}\eta \; - \; gh\,\partial_{xx}\eta \; = \; 0 \tag{55}$$

$$\partial_{tt}U \; - \; gh\,\partial_{xx}U \; = \; 0 \tag{56}$$

The solutions to these equations should be twice differentiable in space and time. And yet the elevation and transport displayed in Figures 4 and 5 seem to exhibit cusps, i.e., points where the aforementioned functions are not differentiable in space. This issue needs further investigation.

In an unbounded domain (i.e., $x \in]-\infty,+\infty[$) the solutions to (55)-(56) can be written in the form of the sum of a signal propagating in the direction in which x increases, identified below by superscript "“+", and a signal propagating in the direction in which x decreases, identified below by superscript "“-", i.e.,

$$\eta(t,x) \; = \; \eta^{+}(t,x) \; + \; \eta^{-}(t,x) \; = \; \eta^{+}\left(0,x-\sqrt{gh}\,t\right) \; + \; \eta^{-}\left(0,x+\sqrt{gh}\,t\right) \tag{57}$$

$$U(t,x) \; = \; U^{+}(t,x) \; + \; U^{-}(t,x) \; = \; U^{+}\left(0,x-\sqrt{gh}\,t\right) \; + \; U^{-}\left(0,x+\sqrt{gh}\,t\right) \tag{58}$$

One of the incentives for illustrious mathematician Laurent Schwartz to conceive the theory of distributions (e.g., Schwartz 1997) was to introduce wave equation solutions similar to (57)-(58) that would not be twice differentiable in space, including C^0 or even discontinuous functions.

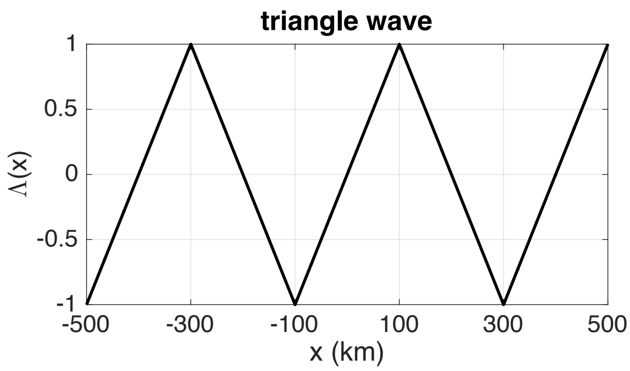

Figure 8. Graphical representation of dimensionless triangle wave (49) in the interval $-500\text{ km} < x < 500\text{ km}$. Its wavelength is 400 km and its amplitude is equal to unity.

The presence of cusps in the elevation and transport profiles should be interpreted in the framework of the theory of distributions. To gain insight into this, it is useful to introduce the following dimensionless triangle wave (Figure 8)

$$\Lambda(x) \; = \; 4\left|\frac{1}{4}+\frac{x}{2L}-\left\lfloor\frac{x}{2L}+\frac{3}{4}\right\rfloor\right| \; - \; 1 \tag{59}$$

where $\lfloor \varsigma \rfloor$ denotes the floor of ς , i.e., the greatest integer less than or equal to ς . Its wavelength is $2L = 400\text{ km}$. It is equivalent to Fourier series

$$\Lambda_f(x) = \sum_{n=1}^{\infty} \frac{8\,(-1)^{n+1}}{\pi^2(2n-1)^2} \sin[(2n-1)\pi x / L] \tag{60}$$

which means that, although $\Lambda(x)$ is C^0 and $\Lambda_f(x)$ is a sum of C^∞ modes, the L^2-norm of their difference is zero. Then, expressions (Figure 9 and Figure 10)

$$\eta(t,x) = \underbrace{\frac{E}{2}\Lambda\left(x-\sqrt{gh}\,t\right)}_{=\eta^+(t)} + \underbrace{\frac{E}{2}\Lambda\left(x+\sqrt{gh}\,t\right)}_{=\eta^-(t)} \tag{61}$$

$$U(t,x) = \underbrace{\frac{\sqrt{gh}\,E}{2}\Lambda\left(x-\sqrt{gh}\,t\right)}_{=U^+(t)} + \underbrace{\left[-\frac{\sqrt{gh}\,E}{2}\Lambda\left(x+\sqrt{gh}\,t\right)\right]}_{=U^-(t)} \tag{62}$$

satisfy (55)-(56) in the sense of the theory of distributions, as well as the initial and boundary conditions of the linear model of external seiching in the lake under consideration. In other words, in the interval $x \in [-L/2, L/2]$, elevation (61) may be viewed as equivalent to (38) or (41), and, by the same token, transport (63) is similar to (39) or (42).

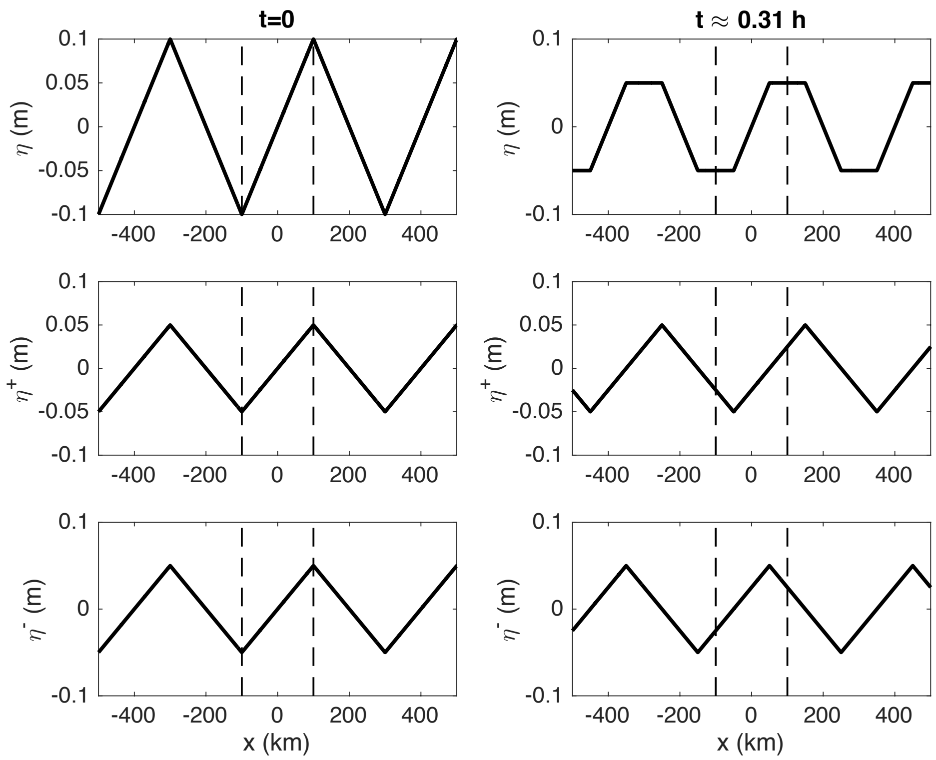

Figure 9. Graphical representation of elevations $\eta(t,x)$, $\eta^+(t,x)$ and $\eta^-(t,x)$ following relation (61). The η^+ triangle wave propagates at speed $\sqrt{gh}$ in the direction in which x increases, whilst η^- propagates in the opposite direction at the same speed. Since $\eta^+(t,x)$ and $\eta^-(t,x)$ have the same amplitude and wavelength $(2L)$, their sum, $\eta(t,x) = \eta^+(t,x) + \eta^-(t,x)$, is a standing wave. The dashed lines represent the boundaries of the lake under consideration herein. These surface elevation waves are also illustrated in an animation (Deleersnijder 2024a).

Solutions exhibiting cusps such as those derived above do not seem to be mentioned in well-known textbooks or review papers dealing primarily or incidentally with seiches (e.g., Fischer et al. 1979, Csanady 1982, Gill 1982, Rabinovich 2010, Cushman-Roisin and Beckers 2011), or in highly sophisticated analytical studies (e.g., Servais 1957, Dobrokhotov et al. 2023). These works, like many others, focus chiefly on eigenmodes of oscillation, which in many, if not all cases are C^{∞} functions, and their sum is hardly ever taken into consideration.

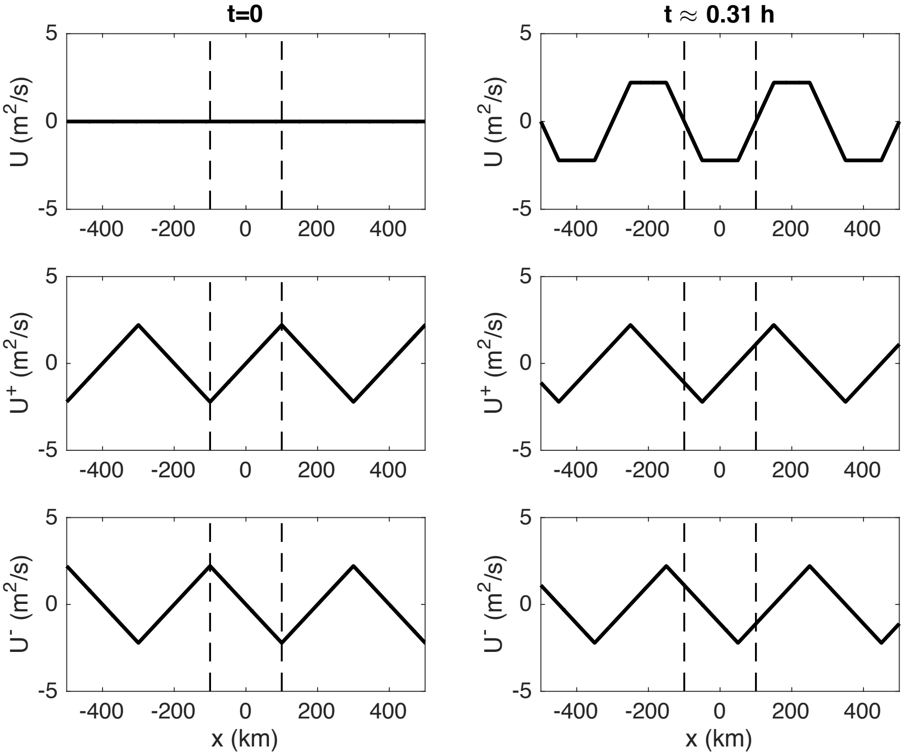

Figure 10. Graphical representation of elevations $U(t,x)$, $U^{+}(t,x)$ and $U^{-}(t,x)$ following relation (62). The U^{+} triangle wave propagates at speed $\sqrt{gh}$ in the direction in which x increases, whilst U^{-} propagates in the opposite direction at the same speed. Since $U^{+}(t,x)$ and $U^{-}(t,x)$ have the same amplitude and wavelength $(2L)$, their sum, $U(t,x)=U^{+}(t,x)+U^{-}(t,x)$, is a standing wave. The dashed lines represent the boundaries of the lake under consideration herein. It is readily seen that transport $U(t,x)$ satisfies the impermeability conditions of these boundaries, i.e., $[U(t,x)]_{x=\pm L/2}=0$. These transport waves are also illustrated in an animation (Deleersnijder 2024a).

It must be stressed that the initial profiles of the elevation and the pycnocline displacement considered above do not satisfy the impermeability conditions of the ends of the lake, which, in the framework of the linearised model, are equivalent to

$$\left[\eta_x\right]_{x=\pm L} = 0 = \left[\eta_x\right]_{x=\pm L} \tag{63}$$

Assuming that the lake is initially motionless, as has been done hitherto, the very reason why the solutions derived above exhibit cusps is related to the nature of the initial condition for the elevation or the pycnocline displacement. Furthermore, a simple inspection of the above mathematical developments indicates that the surface elevation or the pycnocline displacement cannot be a linear function of the space coordinate at all times — although some published schematics might suggest the existence of such solutions.

Initial elevation

$$\eta_0(x) = E\sin(k_1 x) \tag{64}$$

with $k_1 = \pi / L$, is C^∞ and satisfies (63). Then, at any time and position, the elevation and external transport read

$$\eta(t,x) \;=\; E\cos(\omega_1 t)\sin(k_1 x) \tag{65}$$

$$U(t,x) \;=\; -\sqrt{gh}\; E\cos(\omega_1 t)\sin(k_1 x) \tag{66}$$

or, equivalently,

$$\eta(t,x) \;=\; \underbrace{\frac{1}{2}E\sin\left[k_1(x-\sqrt{gh}\;t)\right]}_{=\eta^+(t,x)} \;+\; \underbrace{\frac{1}{2}E\sin\left[k_1(x+\sqrt{gh}\;t)\right]}_{=\eta^-(t,x)} \tag{67}$$

$$U(t,x) \;=\; \underbrace{\frac{\sqrt{gh}}{2}E\sin\left[k_1(x-\sqrt{gh}\;t)\right]}_{=U^+(t,x)} \;+\; \underbrace{\left[-\frac{\sqrt{gh}}{2}E\sin\left[k_1(x+\sqrt{gh}\;t)\right]\right]}_{=U^-(t,x)} \tag{68}$$

with $\omega_1 = \pi\sqrt{gh}\;/L$. These simple expressions, which are C^∞, or similar ones are sometimes used in order to illustrate the dynamics of (external or internal) seiches. For instance, if

$$\eta_0(x) \;=\; \left(\frac{3x}{L}-\frac{4x^3}{L^3}\right)E \tag{69}$$

then the surface elevation is (38) or, equivalently, (41), with

$$E_n \;=\; \frac{2}{L}\int\limits_{-L/2}^{L/2}\eta_0(x)\sin(k_n x)\,dx \;=\; \frac{96\sin(k_n L/2)}{k_n^4\,L^4} \tag{70}$$

Unsurprisingly, the surface elevation field associated with initial condition (64) is very similar to that ensuing from (69) (Figure 11).

The above considerations allow developing the general solution of the equations for external seiches under the assumptions that the related transport is zero at the initial time $(t=0)$. These solutions are built in unbounded domain $x\in]-\infty,+\infty[$. They are the sum of non-dispersive waves of length scale $2L$ propagating in opposite directions at speed $\sqrt{gh}$. The waves propagating in the direction in which x increases (resp. decreases) are identified by superscript "+" (resp. "-"). The relevant algorithm is as follows:

E1. Build the initial elevation in domain $x\in[-L/2,3L/2]$:

$$\hat{\eta}_0(x) \;=\; \begin{cases}\eta_0(x)\,, & -L/2<x<L/2\\ \eta_0(L/2-x) & L/2<x<3L/2\end{cases} \tag{71}$$

E2. Build the initial elevation in domain $x\in]-\infty,+\infty[$:

$$\breve{\eta}_0(x) \;=\; \hat{\eta}(\tilde{x})\;\;,\quad \tilde{x}=x-\left\lfloor\frac{x+L/2}{2L}\right\rfloor(2L) \tag{72}$$

E3. Build the elevation field in domain $x \in]-\infty,+\infty[$:

$$\eta(t,x) = \underbrace{\frac{1}{2}\breve{\eta}_0\left(x-\sqrt{gh}\,t\right)}_{=\eta^+(t,x)} + \underbrace{\frac{1}{2}\breve{\eta}_0\left(x+\sqrt{gh}\,t\right)}_{=\eta^-(t,x)} \tag{73}$$

E4. Build the external mode (or barotropic) transport field in domain $x \in]-\infty,+\infty[$:

$$U(t,x) = \underbrace{\sqrt{gh}\;\eta^+(t,x)}_{=U^+(t,x)} + \underbrace{\left[-\sqrt{gh}\;\eta^-(t,x)\right]}_{=U^-(t,x)} \tag{74}$$

Needless to say, expressions (73)-(74) hold valid in the idealised lake under consideration, i.e., in domain $x \in]-L/2, L+2[$. In particular, transport (74) satisfies the impermeability conditions of both ends of the lake, i.e., $U(t,-L/2) = 0 = U(t,L/2)$.

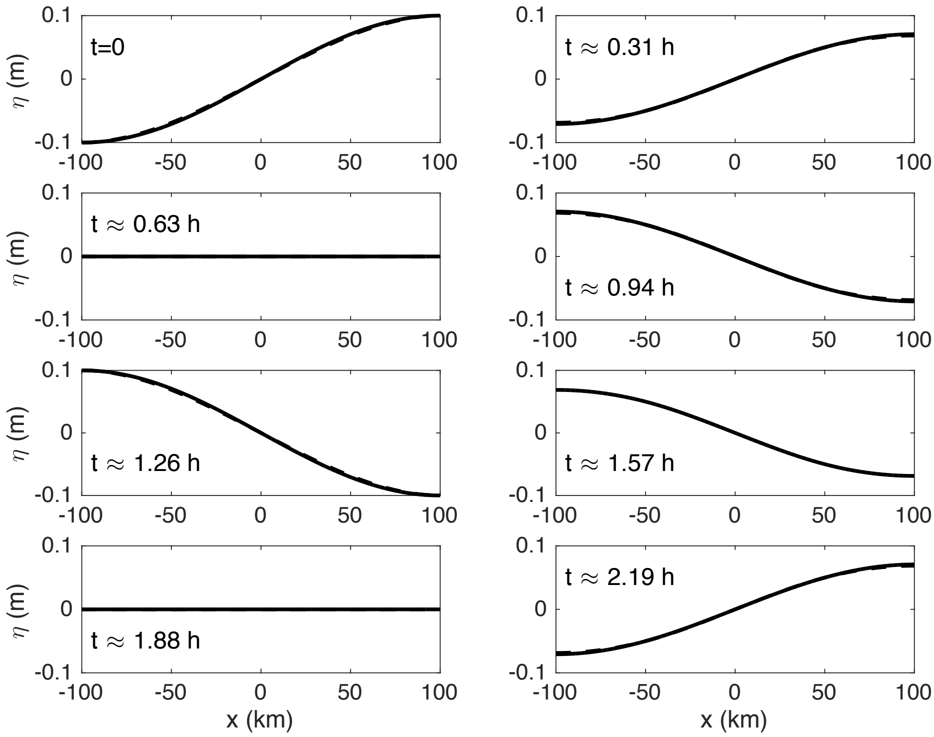

Figure 11. Seiching motion of lake surface elevation $\eta(t,x)$ ensuing from initial conditions (64) (solid curved) and (69) (dashed curve). The length and depth of the lake are $L = 200$ km and $h = 200$ m , respectively. The period of the external seiches represented above is approximately 2.51 hours.

If the initial internal (or baroclinic) transport is zero, then the algorithm for building the general solution of the equations for internal seiches is similar to that related to external seiches. The following steps are to be performed:

I1. Build the initial pycnocline displacement in domain $x \in [-L/2, 3L/2]$:

$$\hat{\xi}_0(x) = \begin{cases} \xi_0(x), & -L/2 < x < L/2 \\ \xi_0(L/2-x) & L/2 < x < 3L/2 \end{cases} \tag{75}$$

I2. Build the initial pycnocline displacement in domain $x \in]-\infty,+\infty[$:

$$\breve{\xi}_0(x) \;=\; \hat{\xi}_0(\tilde{x}) \;\;,\quad \tilde{x} = x - \left\lfloor \frac{x+L/2}{2L} \right\rfloor (2L) \tag{76}$$

I3. Build the pycnocline displacement field in domain $x \in]-\infty,+\infty[$:

$$\xi(t,x) \;=\; \underbrace{\frac{1}{2}\,\breve{\xi}_0\!\left(x-\sqrt{g'h'}\,t\right)}_{=\xi^+(t,x)} \;+\; \underbrace{\frac{1}{2}\,\breve{\xi}_0\!\left(x+\sqrt{g'h'}\,t\right)}_{=\xi^-(t,x)} \tag{77}$$

I4. Build the internal mode (or baroclinic) transport field in domain $x \in]-\infty,+\infty[$:

$$U'(t,x) \;=\; \underbrace{\sqrt{g'h'}\;\xi^+(t,x)}_{=U'^+(t,x)} \;+\; \underbrace{\left[-\sqrt{g'h'}\;\xi^-(t,x)\right]}_{=U'^-(t,x)} \tag{78}$$

The phase speed of the internal mode waves is $\sqrt{g'h'}$, which is much smaller than the speed ($\sqrt{gh}$) of the external mode waves (Figure 3). Expressions (77)-(78) hold valid in the idealised lake under consideration, i.e., in domain $x \in]-L/2, L+2[$. In particular, transport (78) satisfies the impermeability conditions of both ends of the lake, i.e., $U'(t,-L/2) = 0 = U'(t,L/2)$.

Wind-driven external and internal modes

Free oscillations have been examined above. This approach is not concerned with forcings. Therefore, for the sake of completeness, it is necessary to study forced oscillations, the most plausible driving force of which is surface wind stress. Accordingly, the present one-dimensional, linear, two-layer model is modified to take into account constant wind stress $\tau^s\ (>0)$, which is associated with friction velocity

$$u_* \;=\; \sqrt{\frac{\tau^s}{\rho^s}} \tag{79}$$

Then, the equations governing the external mode are

$$\partial_t \eta \;+\; \partial_x U \;=\; 0 \tag{80}$$

$$\partial_t U \;=\; -\,gh\partial_x \eta \;+\; u_*^2 \tag{81}$$

whilst those of the internal mode read

$$\partial_t \xi \;+\; \partial_x U' \;=\; 0 \tag{82}$$

$$\partial_t U' \;=\; -\,g'h'\partial_x \xi \;+\; \frac{h^b}{h} u_*^2 \tag{83}$$

At the initial instant $(t=0)$, all of the state variables are zero, i.e.,

$$\left[\eta(t,x)\right]_{t=0} = \;0\; = \left[\xi(t,x)\right]_{t=0} \;\;,\quad \left[U(t,x)\right]_{t=0} = \;0\; = \left[U'(t,x)\right]_{t=0} \tag{84}$$

Accordingly, the surface wind stress is assumed to be applied abruptly on the lake that is initially motionless. The values of the model parameters are as follows:

$$L = 2\times10^5 \text{ m} \;\;,\quad h = 200 \text{ m} \;\;,\quad h^s = 20 \text{ m} \;\;,\quad g = 9.81\,\text{m/s}^2 \;\;,\quad \varepsilon = 10^{-2} \tag{85a}$$

and

$$u_* = 10^{-2} \text{ m/s} \tag{85b}$$

which corresponds to a wind speed of the order of 10 m/s (e.g., Smith and Banke 1975).

The lake surface elevation that obeys (80), (81) and (84) is

$$\eta(t,x) = \frac{2Ex}{L} - \sum_{n=1}^{\infty} E_n \cos(\omega_n t)\sin(k_n x) \tag{86}$$

with

$$E_n = \frac{8(-1)^{n+1}}{\pi^2(2n-1)^2} E \ , \quad E = \frac{L u_*^2}{2gh} \tag{87}$$

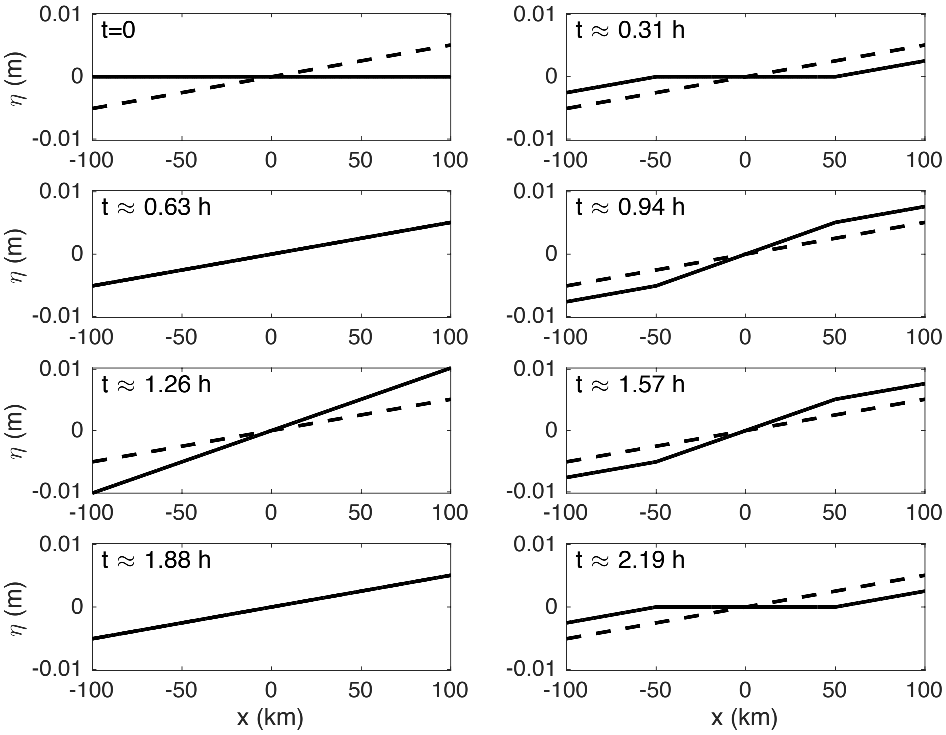

Figure 12. Wind-driven surface elevation $\eta(t,x)$ according to (86) and (87) (solid line) and steady-state response to the surface forcing, i.e., $2Ex/L$ (dashed line). The length and depth of the lake are $L = 200 \text{ km}$ and $h = 200 \text{ m}$, respectively. The unperturbed thickness of the surface layer is $h^s = 20 \text{ m}$. The relative density difference between the two layers is $\varepsilon = 10^{-2}$. The period of the surface oscillations is approximately 2.51 hours. These surface elevation oscillations are also illustrated in an animation (Deleersnijder 2024b).

Clearly, the surface elevation is the sum of the steady state response to the surface forcing, $2Ex/L$, and seiches rather similar to those studied in the preceding section (Figure 12). Their period is $2L/\sqrt{gh}$. Elevation (85) satisfies inequalities

$$\begin{cases} 0 < x < L/2: \ 0 \le \eta(t,x) \le 4Ex/L \\ -L/2 < x < 0: \ 4Ex/L \le \eta(t,x) \le 0 \end{cases} \tag{88}$$

The external mode transport consists only of seiching motion, i.e.,

$$U(t,x) = \sqrt{gh} \sum_{n=1}^{\infty} E_n \sin(\omega_n t) \cos(k_n x) \tag{89}$$

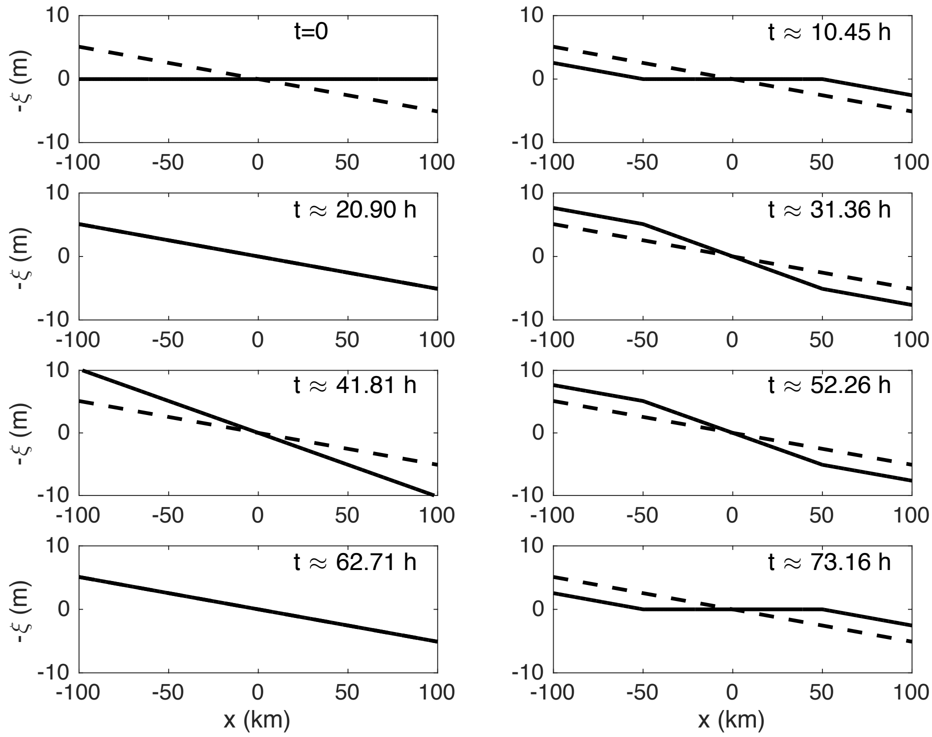

Figure 13. Wind-driven pycnocline displacement, $-\xi(t,x)$, according to (90) and (92) (solid line) and steady-state response to the surface forcing, $-2\Xi x/L$ (dashed line). The length and depth of the lake are $L = 200$ km and $h = 200$ m, respectively. The unperturbed thickness of the surface layer is $h^s = 20$ m. The relative density difference between the two layers is $\varepsilon = 10^{-2}$. The period of the thermocline oscillations is approximately 83.62 hours. These pycnocline oscillations are also illustrated in an animation (Deleersnijder 2024b).

Unsurprisingly, the internal mode state variables satisfy expressing bearing similarities with those of the external mode, i.e.,

$$\xi(t,x) = \frac{2\Xi x}{L} - \sum_{n=1}^{\infty} \Xi_n \cos(\omega'_n t) \sin(k_n x) \tag{90}$$

$$U'(t,x) = \sqrt{g'h'} \sum_{n=1}^{\infty} \Xi_n \sin(\omega'_n t) \cos(k_n x) \tag{91}$$

with

$$\Xi_n = \frac{8(-1)^{n+1}}{\pi^2(2n-1)^2}\,\Xi \quad , \quad \Xi = \frac{L(u_*)^2}{2g'h^s} \tag{92}$$

The period of the thermocline oscillations (Figure 13) is $2L/\sqrt{g'h'}$, which is much larger than the period of the surface oscillations.

As with the free oscillations, the wind-driven ones are characterised by continuous piecewise linear state variables — which exhibit cusps.

Possible misconceptions

There is no doubt that the theory of standing waves is instrumental in comprehending the nature and dynamics of external or internal seiches. This is clear since at least Forel (1876). Though this Author seemed to have little or no knowledge of the mathematics of waves (whose inception probably dates back to the seventeenth century), he correctly described most of the key features of external seiches (which also apply to internal ones). Their period is independent of the position and the amplitude of the oscillations. The latter is maximum at the ends of the water body and negligible in its middle. When the oscillation is at its peak at one end of the domain, it is at its trough at the opposite end. There are, however, possible misconceptions about the concept of seiches. Some of them are as follows:

M1. Had Duke of Normandy William the Conqueror not invaded Britain in 1066, approximately one third of today's English words would not have originated from Old French, eventually leading to a number of so-called false friends. The word “seiche” is, to a certain degree, a false friend, but, for once, the ultimate blame cannot be put on the most famous Duke of Normandy[4]. In today's French, the word “seiche” occasionally refers to the oscillatory phenomena dealt with herein, but, for the general public, “une seiche” is most likely to be a marine animal such as that depicted in Figure 14.

Figure 14. Photograph of a common cuttlefish (*Sepia officinalis*)[5], a cephalopod mollusc, which is named “seiche commune” in French. Like octopuses, it has eight arms. Its length is of the order of a few tens of centimetres.

[4] The author of the present working note is neither an historian nor a linguist. As a consequence, this view may well be completely wrong.

[5] Attribution: Hans Hillewaert. Licence: CC BY-SA 4.0. Source: https://commons.wikimedia.org/wiki/File:Sepia_officinalis_(aquarium).jpg (last viewed on 29 August 2024)

M2. Several widely-accessible cartoons seem to suggest that the seiching displacement of the surface or the pycnocline of the water body of interest is a linear function of the horizontal coordinate(s) (Figure 15). The present working note shows that this interpretation may be somewhat misleading. A novel cartoon is suggested (Figure 16), which is in line with the results obtained herein. Unfortunately, it lacks simplicity.

M3. Simple, if not simplistic descriptions of external and internal seiches do not always point clearly to the huge difference between their timescales. As is seen herein, the period of the former is generally several orders of magnitude smaller than that of the latter. Of course, this remark does not apply to geophysical and environmental publications made by qualified authors.

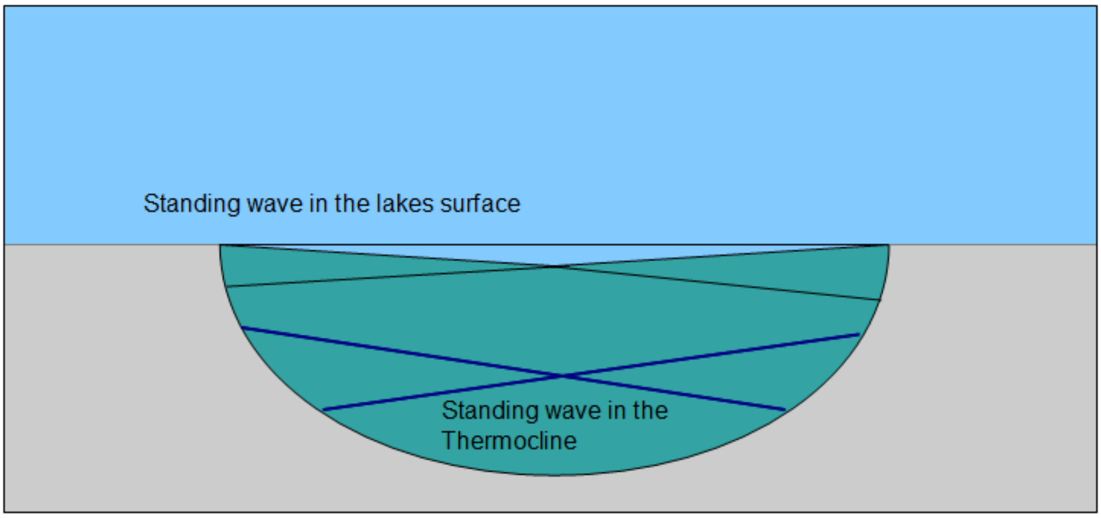

Figure 15. Illustration[6] of standing wave motion (i.e., seiches) of the surface of a lake and its thermocline.

M4. Some may believe that linearising the governing equations of the two-layer model could jeopardise volume and energy conservation, which is guaranteed in the non-linear model. This is not so, as is seen in the Appendix A. Volume and energy are conserved in both types of models.

M5. It is tempting to systematically regard lake-wide surface or pycnocline oscillations as seiches. However, there are also oscillations that are a direct response to the surface wind stress variations. For instance, Gourgue et al. (2011) argued that a large fraction of the oscillations of Lake Tanganyika's thermocline are wind-forced oscillations rather than free ones.

M6. Whether or not the analytical solutions derived above could be relevant test cases for the

[6] Attribution: Frankemann. Licence: CC BY-SA 3.0. Source: lower panel of figure https://commons.wikimedia.org/wiki/File:Illustration_of_the_phenomenon_of_seiches.png (last viewed on 29 August 2024)

mode splitting of a three-dimensional model is far from clear. This is because ensuring that the pycnocline of a level model remains sharp is far from easy and may require the implementation of a adaptive grid system (e.g., Delandmeter 2018). On the other hand, it may also be worth considering internal waves associated with a continuous (reference) density profile (Appendix B).

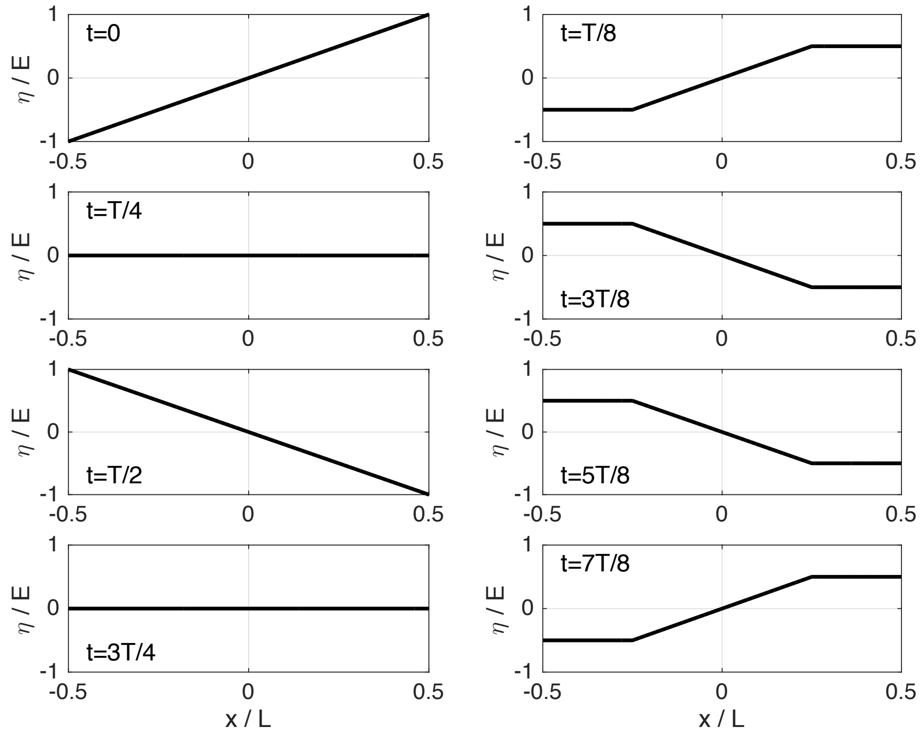

Figure 16. Schematic representation of the seiching motion of a (one-dimensional) lake surface, which is in line with the results obtained in the present working note. The lake surface elevation is denoted $\eta(t,x)$, whilst positive constants L, E and T represent the length of the lake, the amplitude of the seiche and the period of the latter, respectively. A similar type of representation may be made for a thermocline seiche.

Acknowledgements. This working note is a mere attempt at formulating in some details a suggestion formulated by Professor Jean-Marie Beckers (personal communication, 30 May 2024). Ishan Deleersnijder made the animations film1.mp4 and film2.mp4; his help is gratefully acknowledged. Dr Pierre-Denis Plisnier provided useful comments on several aspects of this working note. Dr Jonathan Lambrechts and Florian De Bel contributed to the analytical developments of Appendix B.

Appendix A: Energy budget

The volume of the upper layer, V^s, and that of the lower layer, V^b, are

$$V^s = \int_{\mathcal{S}} H^s \, d\mathcal{S} = \int_{\mathcal{S}} (h^s + \eta + \xi) \, d\mathcal{S} \quad , \quad V^b = \int_{\mathcal{S}} H^b \, d\mathcal{S} = \int_{\mathcal{S}} (h^b - \xi) \, d\mathcal{S} \tag{A.1}$$

where $\mathcal{S}$ denotes the planar extent of the domain of interest, whole lateral boundary, $\mathcal{L}$, is vertical. The water-air interface, the pycnocline and the lateral boundary are assumed to be impermeable. The impermeability condition of the latter boundary reads

$$\left[\mathbf{u}^s \bullet \mathbf{n}\right]_{(x,y)\in\mathcal{L}} = 0 = \left[\mathbf{u}^b \bullet \mathbf{n}\right]_{(x,y)\in\mathcal{L}} \tag{A.2}$$

where unit vector **n** is normal to $\mathcal{L}$. Clearly, the abovementioned volumes as well as the total water volume, $V = V^s + V^b$, must be time-independent. These properties may also be deduced from the integration over the domain of interest of continuity equations (1) and (3), i.e.,

$$\begin{aligned} \frac{dV^s}{dt} &= \frac{d}{dt}\int_{\mathcal{S}} (h^s + \eta + \xi) \, d\mathcal{S} = \int_{\mathcal{S}} \frac{\partial}{\partial t}(\eta + \xi) \, d\mathcal{S} \\ &= \underbrace{-\int_{\mathcal{S}} \nabla \bullet \mathbf{U}^s \, d\mathcal{S} = -\int_{\mathcal{L}} \mathbf{U}^s \bullet \mathbf{n} \, d\mathcal{L}}_{\text{using the divergence theorem}} = 0 \end{aligned} \tag{A.3}$$

$$\begin{aligned} \frac{dV^b}{dt} &= \frac{d}{dt}\int_{\mathcal{S}} (h^b - \xi) \, d\mathcal{S} = \int_{\mathcal{S}} \frac{\partial}{\partial t}(-\xi) \, d\mathcal{S} \\ &= \underbrace{-\int_{\mathcal{S}} \nabla \bullet \mathbf{U}^b \, d\mathcal{S} = -\int_{\mathcal{L}} \mathbf{U}^b \bullet \mathbf{n} \, d\mathcal{L}}_{\text{using the divergence theorem}} = 0 \end{aligned} \tag{A.4}$$

$$\frac{dV}{dt} = \frac{d}{dt}(V^s + V^b) = 0 \tag{A.5}$$

The kinetic energy of the surface layer, K^s, and that of the lower layer, K^b, read

$$K^s = \int_{\mathcal{S}} \frac{\rho^s H^s \left|\mathbf{u}^s\right|^2}{2} d\mathcal{S} \quad , \quad K^b = \int_{\mathcal{S}} \frac{\rho^b H^b \left|\mathbf{u}^b\right|^2}{2} d\mathcal{S} \quad , \quad K = K^s + K^b \tag{A.6}$$

where K is the total kinetic energy of the system under study. Manipulating governing equations (1)-(4) yields

$$\frac{dK^s}{dt} = -\frac{d}{dt}\int_{\mathcal{S}} \frac{g\rho^s \eta^2}{2} d\mathcal{S} - \int_{\mathcal{S}} g\rho^s \eta \partial_t \xi \, d\mathcal{S} + \int_{\mathcal{S}} \boldsymbol{\tau}^s \bullet \mathbf{u}^s \, d\mathcal{S} \tag{A.7}$$

$$\frac{dK^b}{dt} = -\frac{d}{dt}\int_{\mathcal{S}} \frac{g(\rho^b - \rho^s)\xi^2}{2} d\mathcal{S} + \int_{\mathcal{S}} g\rho^s \eta \partial_t \xi \, d\mathcal{S} \tag{A.8}$$

and, hence,

$$\frac{dK}{dt} = -\frac{d}{dt}\int_{\mathcal{S}} \frac{g\rho^s \eta^2 + g(\rho^b - \rho^s)\xi^2}{2} d\mathcal{S} + \int_{\mathcal{S}} \boldsymbol{\tau}^s \bullet \mathbf{u}^s \, d\mathcal{S} \tag{A.9}$$

The Coriolis force does not work since it is orthogonal to the velocity (or transport). As a consequence, this force has no impact on the evolution of the kinetic energy.

The potential gravitational energies read

$$U^s = \int_{\mathcal{S}} \int_{-h^s-\xi}^{\eta} g\rho^s (z-Z)\, d\mathcal{S} \quad , \quad U^b = \int_{\mathcal{S}} \int_{-h^s-h^b}^{-h^s-\xi} g\rho^b (z-Z)\, d\mathcal{S} \quad , \quad U = U^s + U^b \qquad \text{(A.10)}$$

where Z is the altitude at which the potential energy is arbitrarily prescribed to be zero. As is seen below, the value of Z, is unimportant as far as the exchange of energy between the two layers of the system are concerned. Manipulating governing equation (1)-(4) leads to

$$\frac{dU^s}{dt} = \frac{d}{dt}\int_{\mathcal{S}} \frac{g\rho^s\eta^2 - g\rho^s\xi^2}{2}\, d\mathcal{S} \qquad \text{(A.11)}$$

$$\frac{dU^b}{dt} = \frac{d}{dt}\int_{\mathcal{S}} \frac{g\rho^b\xi^2}{2}\, d\mathcal{S} \qquad \text{(A.12)}$$

$$\frac{dU}{dt} = \frac{d}{dt}\int_{\mathcal{S}} \frac{g\rho^s\eta^2 + g(\rho^b - \rho^s)\xi^2}{2}\, d\mathcal{S} \qquad \text{(A.13)}$$

Using (A.9) and (A.13) yields

$$\frac{d}{dt}(K+U) = \int_{\mathcal{S}} \boldsymbol{\tau}^s \bullet \mathbf{u}^s\, d\mathcal{S} \qquad \text{(A.14)}$$

Owing to the motion of the surface and the pycnocline, the upper and lower layers exchange energy. However, the evolution of the mechanical energy of the system (i.e., the sum of the kinetic and potential energies) is due to the wind stress alone (Figure A.1): in the absence of surface forcing, the mechanical energy of the system is conserved. This is unsurprising since the system is a non-dissipative one.

Remarkably, relations (A.7)-(A.14) remain valid for linearised governing equations (5)-(8a), provided H^s and H^b and replaced by h^s and h^b, respectively, in definitions (A.6) of the kinetic energies.

The two-layer model dealt with herein does not fit in with the Boussinesq approximation. To apply the latter to the present model, upper- and lower-layer momentum equations (2) and (4) must be simplified to

$$\rho_\bullet \left[\partial_t \mathbf{U}^s + \nabla \bullet \left(\mathbf{U}^s\mathbf{U}^s / H^s\right) + f\,\mathbf{e}_z \times \mathbf{U}^s\right] = -g\rho^s H^s \nabla\eta + \boldsymbol{\tau}^s \qquad \text{(A.15)}$$

$$\rho_\bullet \left[\partial_t \mathbf{U}^b + \nabla \bullet \left(\mathbf{U}^b\mathbf{U}^b / H^b\right) + f\,\mathbf{e}_z \times \mathbf{U}^b\right] = -g\rho^b H^b \nabla\eta + g(\rho^b - \rho^s) H^b \nabla(\eta+\xi) \qquad \text{(A.16)}$$

where constant $\rho_\bullet$ denotes the (Boussinesq) reference density, whose value must obviously be close to ρ^s and ρ^b. A natural choice could be $\rho_\bullet = (\rho^s + \rho^b)/2$. Furthermore, kinetic energies (A.6) should transform to (e.g., Deleersnijder 2025)

$$K^s = \int_{\mathcal{S}} \frac{\rho_\bullet H^s |\mathbf{u}^s|^2}{2}\, d\mathcal{S} \quad , \quad K^b = \int_{\mathcal{S}} \frac{\rho_\bullet H^b |\mathbf{u}^b|^2}{2}\, d\mathcal{S} \quad , \quad K = K^s + K^b \qquad \text{(A.17)}$$

No modifications of (A.7)-(A.14) and Figure (A.1) are needed.

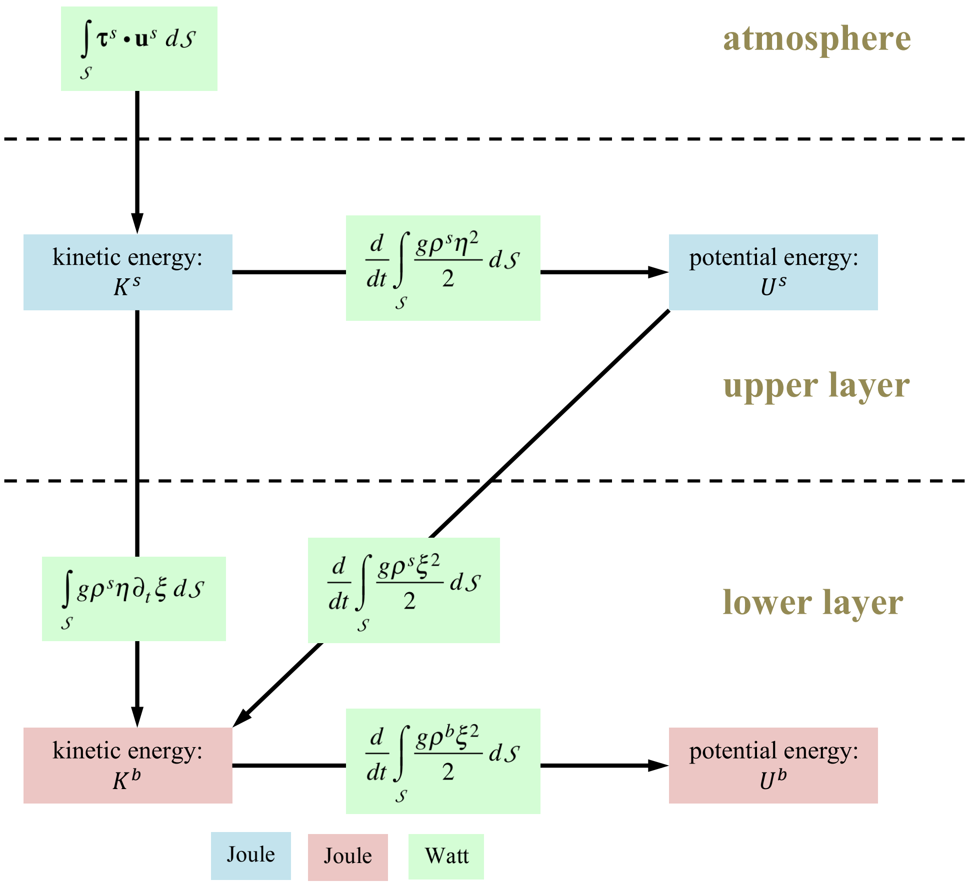

Figure A.1. Energy budget of the non-dissipative, two-layer system under study, assuming that the lateral boundaries of domain of interest ($\mathcal{S}$) are impermeable. The blue- and pink-shaded boxes are energies, which can be measured in Joule. The expressions in the green-shaded boxes represent energy fluxes (whose physical dimension is energy/time and the related units can be Joule/second, i.e., Watt); each arrow indicates the direction of the related energy flux under the hypothesis that the expression in the green-shaded box is positive. None of the energy flux is positive definitive.

Appendix B: Hydrostatic internal waves

We aim to study hydrostatic internal waves in a horizontally unbounded domain of constant depth h $(-h \le z \le 0)$. The relevant state variables are horizontal velocity $\mathbf{u}(t,\mathbf{x},z)$, vertical velocity $w(t,\mathbf{x},z)$, pressure $p(t,\mathbf{x},z)$ and density $\rho(t,\mathbf{x},z)$. We must first define a motionless, hydrostatic reference state (whose state variables are identified by superscript "0"), i.e.,

$$\mathbf{u}^0 = 0\,, \quad w^0 = 0\,, \quad \frac{d}{dz} p^0(z) = -\rho^0(z)\, g \tag{B.1}$$

Brunt-Väisälä frequency $N(z)$, which characterises the reference state stratification, satisfies

$$N^2(z) = -\frac{g}{\rho_\bullet}\frac{d}{dz}\rho_0(z) \tag{B.2}$$

Then, time-dependent, three-dimensional perturbations (identified by superscript "1") of the reference state are taken into consideration, leading to

$$\begin{cases} \mathbf{u}(t,\mathbf{x},z) = \mathbf{u}^0 + \mathbf{u}^1(t,\mathbf{x},z) = \mathbf{u}^1(t,\mathbf{x},z) \ , \quad w(t,\mathbf{x},z) = w^0 + w^1(t,\mathbf{x},z) = w^1(t,\mathbf{x},z) \\ p(t,\mathbf{x},z) = p^0(z) + p^1(t,\mathbf{x},z) \ , \quad \rho(t,\mathbf{x},z) = \rho^0(z) + \rho^1(t,\mathbf{x},z) \end{cases} \tag{B.3}$$

The linearised, non-dissipative equations governing the abovementioned perturbations read (after dropping superscripts "1" for notational simplicity)

$$\nabla \bullet \mathbf{u} + \partial_z w = 0 \tag{B.4}$$

$$\partial_t \mathbf{u} + f\mathbf{e}_z \times \mathbf{u} = -\frac{1}{\rho_\bullet}\nabla p \tag{B.5}$$

$$\partial_z p = -\rho g \tag{B.6}$$

$$\partial_t \rho - \frac{\rho_\bullet}{g}N^2 w = 0 \tag{B.7}$$

The impermeability conditions of the lower and (rigid lid) upper boundaries of the domain are

$$\left[w(t,\mathbf{x},z)\right]_{z=-h} = 0 = \left[w(t,\mathbf{x},z)\right]_{z=0} \tag{B.8}$$

Manipulating (B.4)-(B.7) yields the equation governing the vertical velocity (e.g., LeBlond and Mysak 1978):

$$\partial_{ttzz} w + f^2\partial_{zz} w + N^2\nabla^2 w = 0 \tag{B.9}$$

We substitute into this equation a plane wave solution of the from

$$w(t,\mathbf{x},z) = \mathrm{Re}\left[\tilde{w}(z)e^{i(\omega t - \mathbf{k}\bullet\mathbf{x})}\right] \tag{B.10}$$

leading to

$$\frac{d^2\tilde{w}}{dz^2} + \frac{|\mathbf{k}|^2 N^2}{\omega^2 - f^2}\tilde{w} = 0 \tag{B.11}$$

As the upper and lower boundaries of the domain are impermeable, (B.11) is to be solved under boundary conditions

$$\left[\tilde{w}(z)\right]_{z=-h} = 0 = \left[\tilde{w}(z)\right]_{z=0} \tag{B.12}$$

It is convenient to reformulate ordinary differential problem (B.11)-(B12) by having recourse to the so-called sigma-coordinate. The latter is defined as

$$\sigma = \frac{z+h}{h} \tag{B.13}$$

This dimensionless coordinate is zero at the lower boundary of the water column and is equal to unity at its upper boundary. Substituting (B.13) into (B.11)-(B.12) leads to

$$\frac{d^2\tilde{w}}{d\sigma^2} + \frac{|\mathbf{k}|^2 h^2 N^2}{\omega^2 - f^2}\tilde{w} = 0 \ , \quad \left[\tilde{w}(\sigma)\right]_{\sigma=0} = 0 = \left[\tilde{w}(\sigma)\right]_{\sigma=1} \tag{B.14a}$$

The aspect ratio of the internal waves under consideration is $\delta = h/|\mathbf{k}|^{-1}$, i.e., the ratio of the vertical length scale, h, to the horizontal one, $|\mathbf{k}|^{-1}$. For the hydrostatic equilibrium to be valid, the aspect ratio must be much smaller than unity, otherwise we would need to have recourse to the theory of non-hydrostatic internal waves (e.g., LeBlond and Mysak 1978).

Relations (B.14) constitute a Sturm-Liouville problem. The latter admits a countable set of eigenfunctions, i.e., $\tilde{w}_m(\sigma)$ $(m=1,2,3,...)$, which are associated with eigenvalues

$$\lambda_m = \frac{|\mathbf{k}|^2 h^2 \overline{N^2}}{\omega_m^2 - f^2} = \frac{\delta^2 \overline{N^2}}{\omega_m^2 - f^2} , \quad \lambda_1 < \lambda_2 < \lambda_3 ... \tag{B.15}$$

where

$$\overline{N^2} = \int_0^1 N^2(\sigma)\, d\sigma \tag{B.16}$$

denotes the depth average of $N^2(\sigma)$. The eigenfunctions are orthogonal in the sense that they satisfy

$$\int_0^1 \tilde{w}_l\, \tilde{w}_m\, \varpi\, d\sigma = \begin{cases} =0 & \text{if } l \neq m \\ >0 & \text{if } l = m \end{cases} \tag{B.17}$$

where $\varpi(\sigma) = N^2(\sigma)/\overline{N^2}$ is the relevant weight function. Its depth average obviously is equal to unity. Accordingly, (B14.a) may be rewritten as follows

$$\frac{d^2\tilde{w}_m}{d\sigma^2} + \underbrace{\frac{|\mathbf{k}|^2 h^2 \overline{N^2}}{\omega_m^2 - f^2}}_{=\lambda_m} \underbrace{\frac{N^2}{\overline{N^2}}}_{=\varpi} \tilde{w}_m = 0 , \quad \left[\tilde{w}_m(\sigma)\right]_{\sigma=0} = 0 = \left[\tilde{w}_m(\sigma)\right]_{\sigma=1} \tag{B.14b}$$

with $m = 1,2,3,...$

Combining (B.2) and (B.16) allows introducing the (Boussinesq version of the) relative density difference between lower and upper boundaries of the water column,

$$\varepsilon \triangleq \frac{h}{g}\overline{N^2} = -\frac{\left[\rho(\sigma)\right]_{\sigma=0}^{\sigma=1}}{\rho_\bullet} = \frac{\overbrace{\rho(\sigma=0)}^{\triangleq \rho^b} - \overbrace{\rho(\sigma=1)}^{\triangleq \rho^s}}{\rho_\bullet} = \frac{\rho^b - \rho^s}{\rho_\bullet} \tag{B.18}$$

and the associated reduced gravitational acceleration, i.e., $g' = \varepsilon g$. Setting $h_m = h/\lambda_m$, the dispersion relation of the internal wave under study may be derived from (B.15):

$$\omega_m^2 = f^2 + g' h_m |\mathbf{k}|^2 \tag{B.19}$$

Then, the phase speed of the *m*-th mode reads

$$\left|\mathbf{C}_{p,m}\right| = \sqrt{g' h_m} \sqrt{1 + \frac{|\mathbf{k}|^{-2}}{\left(R_m\right)^2}} \tag{B.20}$$

where $R_m = \sqrt{g' h_m}/|f|$ is the (internal) Rossby radius of deformation relevant to the *m*-th mode, the value of which decreases as the order of the mode (m) increases.

The dispersion relation for the external inertia-gravity waves is mathematically similar to that of the two-layer model internal waves and that of the hydrostatic internal waves in the continuous model. This is unsurprising, for all the processes under consideration are plane waves associated with the displacement of iso-density surfaces on the *f*-plane under the influence of the same restoring force, i.e., the weight of the fluid parcels.

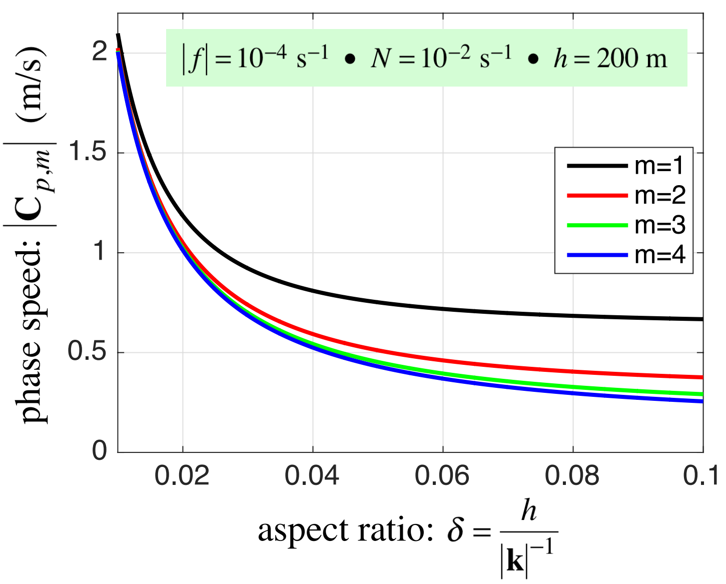

Figure B.1. Phase speed of the first four internal wave modes $(m = 1,2,3,4)$ for a range of plausible values of aspect ratio $\delta = h/|\mathbf{k}|^{-1}$. The latter must be much smaller than unity for the hydrostatic equilibrium to hold valid. The values of Coriolis parameter f, Brunt-Väisälä frequency N and water column depth h are indicated in the upper part of the figure. They are thought to be rather realistic. The phase speed can be of the same order of magnitude as the water velocity, i.e., roughly speaking, 1 m/s .

If the Brunt-Väsäilä frequency is constant (i.e., $N = const.$), the weight function is identically equal to unity $(\varpi = 1)$. Furthermore, the m-th mode eigenvalue, angular frequency, internal Rossby radius of deformation and phase speed satisfy

$$\begin{aligned} \lambda_m &= m^2\pi^2 \quad , \quad \omega_m^2 = f^2 + \frac{N^2 h^2 |\mathbf{k}|^2}{m^2\pi^2} \\ R_m &= \frac{Nh}{\sqrt{\lambda_m}\,|f|} \quad , \quad \left|\mathbf{C}_{p,m}\right| = \frac{Nh}{m\pi}\sqrt{1 + \frac{|\mathbf{k}|^{-2}}{(R_m)^2}} \end{aligned} \tag{B.21}$$

The value of the phase speed $(\propto Nh)$ can be of the same order of magnitude as the water velocity, i.e., roughly speaking, 1 m/s (Figure B.1). This is why internal waves should not be ignored in the analysis of the numerical aspects of three-dimensional models. This, however, is likely to a daunting task, since most, if not all the discrete equations of the model must be taken into consideration. In other words, we cannot simply focus on one discrete equation or tackle a couple of them as most authors have done so far. Furthermore, it is probably desirable that the impact of the lower and upper boundaries of the domain must be accounted for, thereby precluding the application of von Neumann's analysis (e.g., Crank and Nicolson 1947, Isaacson and Keller 1966) or a version thereof adapted to unstructured meshes (e.g., Bernard et al. 2008).

The eigenfuctions are of the form

$$\tilde{w}_m(\sigma) \;=\; 2W_m \sin\!\left(\sqrt{\lambda_m}\,\sigma\right) \;=\; 2W_m \sin(m\pi\sigma) \tag{B.22}$$

where constant W_m, whose physical dimensional is length/time, is such that

$$\int_0^1 \tilde{w}_m^2 \, d\sigma \;=\; W_m^2 \tag{B.23}$$

Clearly, the L^2-norm of $\tilde{w}_m / W_m$ is identically equal to unity.

Equation (B.14a) may be discretised as follows:

$$\frac{\widehat{w}_{j+1} - 2\widehat{w}_j + \widehat{w}_{j-1}}{\Delta\sigma^2} + \frac{|\mathbf{k}|^2 h^2 N^2}{\omega^2 - f^2}\widehat{w}_j \;=\; 0 \;\;, \quad \widehat{w}_0 = 0 = \widehat{w}_J \tag{B.24}$$

with $\widehat{w}_j = \widehat{w}(\sigma_j)$ and $\sigma_j = j\Delta\sigma$ ($j = 0,1,2...J$). Clearly, J is the number of discrete levels and $\Delta\sigma = J^{-1}$ is the vertical increment in the sigma-space. It must be stressed that the number of modes that can be represented in the framework of the discrete problem satisfies $m \le J-1$.

The solution to difference problem (B.24) reads (e.g., Bender and Orszag 1978)

$$\widehat{w}_j \;=\; 2\widehat{W}\,\sin\!\left(\sqrt{\lambda_m}\,\sigma_j\right) \tag{B.25}$$

where $\widehat{W}$ is a relevant constant. The eigenvalues associated with the present discrete problem, $\widehat{\lambda}_m$, obey $\widehat{\lambda}_m < \lambda_m$ and

$$\widehat{\lambda}_m \;=\; 2\,\frac{1-\cos(m\pi\Delta\sigma)}{\Delta\sigma^2} \;\sim\; \underbrace{m^2\pi^2}_{=\lambda_m} \;-\; \frac{m^4\pi^4}{12}\Delta\sigma^2 \;\;, \quad \Delta\sigma \to 0 \tag{B.26}$$

This leads to

$$\widehat{\omega}_m^2 = f^2 + \frac{N^2 h^2 |\mathbf{k}|^2}{\widehat{\lambda}_m} \;\;, \quad \left|\widehat{\mathbf{C}}_{p,m}\right| = \frac{Nh}{\sqrt{\widehat{\lambda}_m}}\sqrt{1 + \frac{|\mathbf{k}|^{-2}}{\left(\widehat{R}_m\right)^2}} \;\;, \quad \widehat{R}_m = \frac{Nh}{\sqrt{\widehat{\lambda}_m}\,|f|} \tag{B.27}$$

The phase speed satisfies

$$\left|\widehat{\mathbf{C}}_{p,m}\right| \;>\; \left|\mathbf{C}_{p,m}\right| \tag{B.28}$$

which is in clear contradiction with Deleersnijder (1992), who obtained $\left|\widehat{\mathbf{C}}_{p,m}\right| < \left|\mathbf{C}_{p,m}\right|$ — by means of a different semi-discrete approach. According to Lambrechts and De Bel (personal communication, November 2024), the phase speed of Deleersnijder (1992) is probably closer to that of a full-fledged discrete model and, hence, should be more trustworthy than that derived from (B.24). Clearly, semi-discrete equations can lead to misleading results...

References

Bajo M., I. Medugorac, G. Umgiesser and M. Orlic, 2019, Storm surge and seiche modelling in the Adriatic Sea and the impact of data assimilation, *Quarterly Journal of the Royal Meteorological Society,* 145, 2070-2084

Baretta-Bekker H.G., E. Duursma and B.R. Kuipers, 1998 (2nd ed.), *Encyclopedia of Marine Sciences*, Springer, 357 pages

Beckers J.-M. and E. Deleersnijder, 1993, Stability of a FBTCS scheme applied to the propagation of shallow-water inertia-gravity waves on various space grids, *Journal of Computational Physics*, 108, 95-104

Bender C.M. and S.A. Orszag, 1978, *Advanced Mathematical Methods for Scientists and Engineers*, McGraw-Hill, 593 pages

Bernard P.-E., E. Deleersnijder, V. Legat and J.-F. Remacle, 2008, Dispersion analysis of discontinuous Galerkin schemes applied to Poincaré, Kelvin and Rossby waves, *Journal of Scientific Computing*, 34, 26-47

Blumberg A.F. and G.L. Mellor, 1987, A description of a three-dimensional coastal ocean circulation model, in: *Three Dimensional Coastal Ocean Models* (N.S. Heaps, Ed.), American Geophysical Union, Washington, D.C., pages 1-16

Cerovecki I., M. Orlic and M.C. Hendershott, 1997, Adriatic seiche decay and energy loss to the Mediterranean, *Deep-Sea Research I*, 44, 2007-2029

Coulter G.W. and R.H. Spigel, 1991, Hydrodynamics, in: *Lake Tanganyika and its Life*, G.W. Coulter (ed.), Oxford University Press, London, pages 49-75

Crank J. and P. Nicolson, 1947, A practical method for numerical evaluation of partial differential equations of the heat-conduction type, *Mathematical Proceedings of the Cambridge Philosophical Society, 43*, 50-67

Csanady G.T., 1982, *Circulation in the Coastal Ocean*, Springer, 281 pages

Cushman-Roisin B. and J.-M. Beckers, 2011, *Introduction to Geophysical Fluid Dynamics - Physical and Numerical Aspects*, International Geophysics Series (Vol. 101), Elsevier, 828 pages

de Jong M.P.C. and J.A. Battjes, 2004, Seiches characteristics of Rotterdam Harbour, *Coastal Engineering*, 51, 373-386

de Jong M.P.C., L.H. Holthuijsen and J.A. Battjes, 2003, Generation of seiches by cold fonts over the southern North Sea, *Journal of Geophysical Research*, 108, 3117, doi: 10.1029/2002JC001422

Delandmeter P., J. Lambrechts, V. Legat, V. Vallaeys, J. Naithani, W. Thiery, J.-F. Remacle and E. Deleersnijder, 2018, A fully consistent and conservative vertically adaptive coordinate system for SLIM 3D v0.4 with application to the thermocline oscillations of Lake Tanganyika, *Geoscientific Model Development*, 11, 1161-1179

Deleersnijder E., 1992, *Propagation of internal modes in three-dimensional ocean level models*, Working Note, Université catholique de Louvain, Louvain-la-Neuve, Belgium, 7 pages, available at URL http://hdl.handle.net/2078.1/214937

Deleersnijder E., 2025, *Energy conservation in geophysical and environmental flows under various simplifying assumptions*, Working Note, Université catholique de Louvain, Louvain-la-Neuve, Belgium, in preparation

Deleersnijder I., 2024a, Animation in mp4 format, available at URL https://perso.uclouvain.be/eric.deleersnijder/film1.mp4.zip

Deleersnijder I., 2024b, Animation in mp4 format, available at URL https://perso.uclouvain.be/eric.deleersnijder/film2.mp4.zip

Dobrokhotov S.Y., V.A. Kalinichenko, D.S. Minenkov and V.E. Nazaikinskii, 2023, Asymptotic of long standing waves in one-dimensional pools with shallow banks: theory and experiment, *Fluid Dynamics*, 58, 1213-126

Fischer H.B., E.J. List, R.C.Y. Koh, J. Imberger and N.H. Brooks, 1979, *Mixing in Inland and Coastal Waters,* Academic Press, San Diego, 483 pages

Forel F.-A., 1876, Les Seiches, vagues d'oscillation fixe des lacs, *Annales de Chimie et de Physique*, vol. série 5, t. 9, p. 1-16, available at URL https://archive-ouverte.unige.ch//unige:164434

Gadd A.J., 1978, A split explicit integration scheme for numerical weather prediction, *Quarterly Journal of the Royal Meteorological Society*, 104, 569-582

Gill A.E., 1982, *Atmosphere-Ocean Dynamics*, Academic Press, San Diego, 662 pages

Gourgue O., E. Deleersnijder, V. Legat, E. Marchal and L. White, 2011, Free and forced thermocline oscillations in Lake Tanganyika, in: *Factor Separation in the Atmosphere: Applications and Future Prospects*, P. Alpert and T. Sholokhman (Eds.), Cambridge University Press, pp. 146-162

Higdon R.L. and R.A. de Szoeke, 1997. Barotropic-baroclinic time splitting for ocean circulation modeling, *Journal of Computational Physics*, 135, 30-53

Isaacson E. and H.B. Keller, 1966, *Analysis of Numerical Methods*, John Wiley & Sons, 541 pages

Ishimwe A.P., 2024, *Multi-scale Time Integration Schemes for Three-Dimensional Hydrodynamic Marine Models*, Doctoral dissertation, Louvain School of Engineering, Université catholique de Louvain, Louvain-la-Neuve, Belgium, 132 pages, available at URL http://hdl.handle.net/2078.1/290661

Ishimwe A.P., E. Deleersnijder, V. Legat and J. Lambrechts, 2023, A split-explicit second order Runge-Kutta method for solving 3D hydrodynamic equations, *Ocean Modelling*, 186, 102273, doi: 10.1016/j.ocemod.2023.102273

Ishimwe A.P., E. Deleersnijder, V. Legat and J. Lambrechts, 2025, A multi-scale IMEX second order Runge-Kutta method for 3D hydrodynamic ocean models, *Journal of Computational Physics*, 520, 113482, doi: 10.1016/j.jcp.2024.113482

Killworth P.D., D. Stainforth, D.J. Webb and S.M. Paterson, 1991, The development of a free-surface Bryan-Cox-Semtner ocean model, *Journal of Physical Oceanography*, 21, 1333-1348

Le Roux D.Y., 2012, Spurious inertial oscillations in shallow-water models, *Journal of Computational Physics*, 231, 7959-7987

LeBlond P.H. and L.A. Mysak, 1978, *Waves in the Ocean*, Elsevier Oceanography Series (n° 20), Elsevier, Amsterdam, 602 pages

Mesinger F. and A. Arakawa, 1976, *Numerical Methods Used in Atmospheric Models*, Vol 1., GARP Publications Series No. 17, World Meteorological Organization and International

Council of Scientific Unions, 64 pages[7]

Moore D.W. and S.G.H. Philander, 1977, Finite-difference formulation of a World Ocean model, in: *Advanced Physical Oceanographic Modeling* (J.J. O'Brien, Ed.), Reidel, Dordrecht, pages 187-202

Naithani J., E. Deleersnijder and P.-D. Plisnier, 2002, Origin of intraseasonal variability in Lake Tanganyika, *Geophysical Research Letters*, 29, 10.1029/2002GL015843

Naithani J., E. Deleersnijder and P.-D. Plisnier, 2003, Analysis of wind-induced thermocline oscillations of Lake Tanganyika, *Environmental Fluid Mechanics*, 3, 23-39

Rabinovich A.B., 2010, Seiches and harbor oscillations, in: *Handbook of Coastal and Ocean Engineering* (Y.C. Kim, Ed.), World Scientific Publishing Co., Singapore, pages 193-236

Piccolroaz S. and M. Toffolon, 2018, The fate of Lake Baikal: how climate change may alter deep ventilation in the largest lake on Earth, *Climatic Change*, 150, 181-194

Schwartz L., 1997, *Un Mathématicien aux Prises avec le Siècle*, Editions Odile Jacob, 528 pages

Servais F., 1957, Etude théorique des oscillations libres (seiches) du lac Tanganyika, *Exploration Hydrobiologique du Lac Tanganyika (1946-1947)*, Volume II, Fascicule 3, Institut Royal des Sciences Naturelles de Belgique, Bruxelles, 307 pages

Shchepetkin A.F. and J.C. McWilliams, 2005, The region oceanic modeling system (ROMS): a split-explicit, free-surface, topography-following-coordinate oceanic model, *Ocean Modelling*, 9, 347-404

Smith S.D. and E.G. Banke, 1975, Variation of the sea surface drag coefficient with wind speed, *Quarterly Journal of the Royal Meteorological Society*, 101, 665-673

Smirnov S.V., K.M. Kucher, N.G. Granin and I.V. Sturova, 2014, Seichelike oscillations in Lake Baikal, *Izvestiya, Atmospheric and Oceanic Physics*, 50, 99-102

Svennevig K. et al., 2024, A rockslide-generated tsunami in a Greenland fjord rang Earth for 9 days, *Science*, 385, 1196-1205

Trebitz A.S., 2006, Characterizing seiche and tide-driven daily water level fluctuations affecting coastal ecosystems of the Great Lakes, *Journal of Great Lakes Research*, 32, 102-116

Vallaeys V., T. Kärnä, P. Delandmeter, J. Lambrechts, A.M. Baptista, E. Deleersnijder and E. Hanert, 2018, Discontinuous Galerkin modeling of the Columbia River's coupled estuary-plume dynamics, *Ocean Modelling*, 124, 111-124

van Emmerik T.H.M., A. Rimmer, Y. Lechinsky, K.J.R. Wenke, S. Nussboim and N.C. van de Giesen, Measuring heat balance residual at lake surface using distributed temperature sensing, *Limnology and Oceanography*, 11, 79-80

Vreugdenhil C.B., 1994, *Numerical Methods for Shallow-Water Flow*, Water Science and Technology Library (n° 13), Kluwer Academic Publishers, Dordrecht, 261 pages

Wahl B. an F. Peeters, 2014, Effect of climatic changes on stratification and deep-water

[7] https://oceanrep.geomar.de/id/eprint/40278/1/Mesinger_ArakawaGARP.pdf (last viewed on 27 June 2024)

renewal in Lake Constance assessed by sensitivity studies with a 3D hydrodynamic model, *Limnology and Oceanography*, 59, 1035-1052